Imperial College London

Human adaptive haptic sensing

Gerolamo Carboni

2021

Department of Bioengineering

Imperial College London

Submitted in partial fulfilment of the requirements for the degree of

Doctor of Philosophy of Imperial College London

and the Diploma of Imperial College London

In the loving memory of Mariangela and Mattia Simula.

Summary

How do humans physically interact with the environment or with other humans? It is well known that the nervous system can modify the body's stiffness by selectively cocontracting muscles to shape the mechanical interaction with the environment, but how this influences haptic perception is not known. This thesis examines whether humans can adapt muscles' activation to influence their perception of the physical interaction with the environment. This question is investigated by conducting behavioural experiments using dedicated robotic interfaces to study sensorimotor interactions in the presence of haptic and visual perturbations. Hypotheses about the underlying mechanism are then tested through mathematical modelling and simulations.

Chapter 1 reviews related frameworks and introduces the most relevant questions addressed in this work. Chapter 2 then shows that the central nervous system (CNS) can voluntarily adapt muscle cocontraction to increase haptic sensitivity. In an experiment, participants tracked a randomly moving target with visual noise while being physically guided by a virtual elastic band, where the band's stiffness was controlled by their muscle coactivation. The results show that participants learned to increase cocontraction with visual noise and decrease it when the guidance is incongruent with the visual target. The adaptation law governing the regulation of the body's stiffness by the CNS is then derived through computational modelling. This model is designed to maximise visuo-haptic information while minimising metabolic cost, thus trading off sensory information with energy.

Further, it is shown in Chapter 3 that when the subjects are coupled via a tuneable connection to a robotic guidance designed to hinder their tracking through perturbations at the turning points (where participants physiologically increase cocontraction), they adapted cocontraction to reduce the impact of perturbations on performance. These results highlight the CNS ability to modify the muscle activation patterns to improve performance with minimal effort.

Chapter 4 tests the robustness of human adaptive haptic sensing introduced in the previous chapters for human-human physical interaction. For example, in tango dancing physical

contact provides haptic information of the partner's action required to coordinate the movements. During such physical interactions, should one keep the arms compliant so that the partner can correct the motion, or should one stiffen them to better keep along the planned movement? Using a tracking task in which a dyad is coupled via a rigid connection, subjects readily adapted the compliance of their limb depending on both the accuracy of the partner's and their own movement. The same computational model introduced in Chapter 2 could explain these results and predict the experimentally observed cocontraction adaptation. This suggests that the minimisation of prediction error and energy is a general principle also holding in interpersonal interactions.

Altogether, these findings shed light on how humans can adapt haptic sensing by changing body properties, and propose a novel framework to interpret visuo-haptic perception for interaction with the environment and other humans.

Keywords: human interaction, haptic sensing and perception, body adaptation, visuo-haptic integration.

Statement of Originality

I hereby certify that the work embodied in this thesis is the result of original research, is free of plagiarised materials, and has not been submitted for a higher degree to any other University or Institution.

Copyright Statement

Acknowledgement

First, I would like to thank my supervisor Etienne who has been a true guide over these years. The discussions we had were not only critical to accomplish the work presented in this thesis, but helped me to grow as an individual. Your trust and support "enabled me to develop ideas that at the end somehow worked out"!

To the past and current members of the Human Robotics Group: Aaron, Alexis, Aran, Arash, Atsushi, Camille, Carlo, Donald, Franck, Ildar, Jin, Jonathan, Lucille, Katja, Matjaz, Mike, Nuria, Pakorn, Paul, Pilar, Rejin, Sajeeva, Seung, Sharah, Sofia, Xiaoxiao, Yanan, Yanpei and Ziwei; thanks for the amazing time at Imperial and in London, I am truly grateful to have been alongside you!

To my people in this journey: Rachel and Sebastiano. To José Fernando.

Finally, I would like to thank my family for their unconditional support. Thank you, for teaching me there is a lot to see and touch and feel in this world. And to Mariangela, for keeping me humble.

This thesis is dedicated to you.

Contents

List of Figures

List of Acronyms

ANOVA Analysis of Variance

ART ANOVA Aligned Ranks Transformation ANOVA

BEM Bayesian Error Minimization

CNS Central Nervous System

DAQ Data Acquisition

DoF Degree of Freedom

ECRL Extensor Carpi Radialis Longus

EMG Electromyography

FCR Flexor Carpi Radialis

HSD Honest Significant Difference

OIE Optimal Information and Effort

PNM Planning Noise Minimization

RANOVA Repeated Measures Analysis of Variance

TEM Tracking Error Minimization

List of Symbols

The following list describes several symbols that will be later used within the body of the dissertation

Chapter 2

δ	Haptic reference bias
η	Visual cloud vertical distance to the visual target (Gaussian distribution)
$\eta_{\dot{q}}$	Visual cloud angular velocity (Gaussian distribution)
η_q	Visual cloud angular distance to the visual target (Gaussian distribution)
γ	Metabolic adaptation parameter
$\hat{u}$	Learned value of muscle cocontraction
κ	Connection stiffness
$\overline{u}$	Mean muscle cocontraction over a trial
$\overline{u}_{max}$	Maximum of mean muscle cocontraction over all trials
$\overline{u}_{min}$	Minimum of mean muscle cocontraction over all trials
σ_b	δ dependant haptic noise standard deviation
σ_h	Haptic noise
σ_k	κ dependant haptic noise standard deviation
σ_v	Visual noise standard deviation
τ	Interaction torque
τ_e	Torque of the extensor muscle (regressed against u_e)
τ_f	Torque of the flexor muscle (regressed against u_f)
E	Bayesian prediction error
e	Tracking error
e_h	Haptic error
e_v	Visual error
q	Wrist position (in degrees)
q^*	Visual target position (in degrees)
q_h	Haptic reference position (in degrees)
u	Muscle cocontraction
u_e	EMG signal - Extensor Carpi Radialis Longus

u_f	EMG signal - Flexor Carpi Radialis
u_n	Normalised muscle cocontraction
w_h	Weight associated to visual information
w_v	Weight associated to haptic information

Chapter 3

β	Disturbance level
$\ddot{q}^*$	Visual target acceleration
$\dot{q}^*$	Visual target velocity

Chapter 4

σ_{ko}	Wrist compliance dependant own tracking deviation from planned motion
σ_o	Own visual noise standard deviation
σ_p	Partner's visual noise standard deviation
σ_{vo}	Visual noise dependant own tracking deviation from planned motion
ζ	Metabolic adaptation parameter in PNM model
q_o	Own wrist position (in radians)
q_p	Partner's wrist position (in radians)

Chapter 1 Introduction

The aims of my thesis are to investigate the human capability of tuning haptic information to improve visuo-haptic sensing and to unveil the computational mechanism underlying this process. I explore whether humans can modulate their body properties, specifically their limb viscoelasticity, for improving sensory information during contact with either the environment or other humans. As a related question, I examine the relationship between impedance modulation and vibrotactile information during physical interaction. I address these questions by developing a novel methodology to systematically study the human behaviour through a set of experiments, using dedicated robotic interfaces and state of the art sensors to analyse sensorimotor interactions, as well as computational models and simulations.

1.1 Background and motivation

When interacting with the external environment or with other humans, we gather physical information from a wide variety of sensory receptors located in the skin, muscle spindles and tendons, to plan our next action based on the current perception. Human haptics, the study of human sensing and manipulation through touch [1], is critical for accomplishing most daily activities and generally allow humans to interact with the surrounding environment. Haptics, from the Greek words ἁπτικός (haptikós, able to come into contact with) and ἁπτός (haptós, tangible) according to the Merriam-Webster dictionary, is commonly viewed as a perceptual system provided with sensory inputs by two afferent subsystems, that most

typically involves active manual exploration [2]. Haptic sensing, e.g. when the hand is interacting with an object, it is based on two kinds of sensory information:

- *Kinesthetic information*, using *proprioception* (sense of limbs' position and motion) and forces detected by the sensory receptors in the skin around the joints, tendons, and muscles, combined with driving motor commands.
- *Tactile information*, during contact with objects, propagated through vibrations and mediated by the skin's mechanoreceptors (mostly present in the fingerpad and in the hand in general).

Mainly kinesthetic information is used to control free motion of the hand, without contact with the environment. In contrast, mainly tactile information is used in contact with an object, while is conveyed together with kinesthetic inputs about the limb posture and isometric forces. In fact, the two afferent systems are not strictly segregated but subserve common functions: previous literature highlighted how both tactile and proprioceptive stimulations lead to the activation of very similar cerebral networks. This arises a unified percept of one's own body movements, thus showing that heteromodal areas may contribute to multisensory integrative mechanisms at cortical and subcortical levels [3]. In addition, as found for the *skin deformation feedback*, specific kinds of tactile feedback provide effective haptic information of force, stiffness, and friction comparable to those emerging from kinesthetic sensing, so that cutaneous and kinesthetic sensory cues can be conveniently integrated [4], [5]. Both classes of information are therefore critical ~~relevant~~ to perform robust unconstrained sensory and manipulation tasks [1].

Within the framework of objects' manipulation, the *tool-use function* is an important aspect that has assumed a central role in the way humans interact and shape the surrounding environment. Goal-oriented grasping and objects' manipulation are skills that rely on predictive strategies integrating somatosensory and visual signals with sensory-motor memory systems [6]. Memory representations of physical and task-relevant properties

of the objects together with feedforward mechanisms are crucial when deliberate actions arise from established relationships between afferent patterns and efferent commands (for reference see the *opposition space model*, that takes into account the hand's ability to apply task-related forces while gathering sensory information [7]).

Figure 1-1: **Different kinds of human interactions.** Humans accomplish a wide range of interactions, from complex interactions with the environment like using a chisel for carving a piece of wood, to helping a friend for moving a heavy object or for social interaction.

Early studies also emphasized a neat distinction in tactual experiences when comparing passive and active interactions: in free arm movements the observer tends to focus on the subjective bodily sensations, whereas contact resulting from active exploration guides the observer's attention to properties of the external environment [8]. In fact, the haptic percept depends on the material properties of the environment we interact with. When a finger slides to scan a surface (tactile sensing), the moving contact induces vibrations that activate receptors allowing the brain to identify objects and to perceive information about their properties. The information is conveyed through signals elicited by friction between the skin and the object scanned by the fingertip. The characteristics of the vibrotactile signals give information about the texture features, thus affecting the tactile perception. Previous studies have focused on the relation between the physical characteristics of the surfaces and the detected signals by investigating the correlation between contact-induced vibrations and tactile perception of textures. Vibration spectra measured on the fingers and in the forearm tissues revealed regularities correlated with the scanned surface that were found to change as a function of contact parameters such as roughness,

surface texture, scanning speed [9], [10], thus transmitting information regarding explored and manipulated objects [11]. These results explain the perceptual mismatch between the real roughness and the perceived roughness of a surface that takes place when a subject receives external vibrations hindering its perception [12]. From this perspective, it looks necessary to characterize the vibrotactile signals that drive neural responses for understanding tactile perception, given the non-trivial dependence of skin vibrations with the hand biomechanics [13]. The correlations between vibrotactile sensory information and motor activity may be of broader significance for the control of human interactions than has been previously acknowledged [14]. On the other hand, recent research also showed that the kinesthetic information exchanged while tracking a common target between virtually connected dyads of physically interacting partners depends on the connection stiffness. The tracking performance monotonically improves with a stiffer connection for the worse partner, at the cost the skilled partner's extra effort, thus highlighting how the coupling impedance connecting the partners determines maximum communicated information [15] (Fig. 1-2).

The CNS combines the haptic information gathered through physical interaction with task relevant information obtained by alternative sensory channels to produce a comprehensive reliable estimate. Sensory weighting between different sensory systems (e.g., vision and proprioception) and within the same sensory system (e.g., force and position in proprioception) have been extensively studied [16], [17]. To quantitatively investigate sensory integration, researchers measured the variances associated with the different sensory estimates and then integrate them. A typical model outcome fits the experimental data, implying that one sensory input prevails over the others when the associated variance is lower than that associated with the other estimates [16], [18]–[20]. Further evidence is pointed by a shift in the brain activity from the primary visual cortex to the motor cortex concurrent when altering visual and haptic information reliability [21].

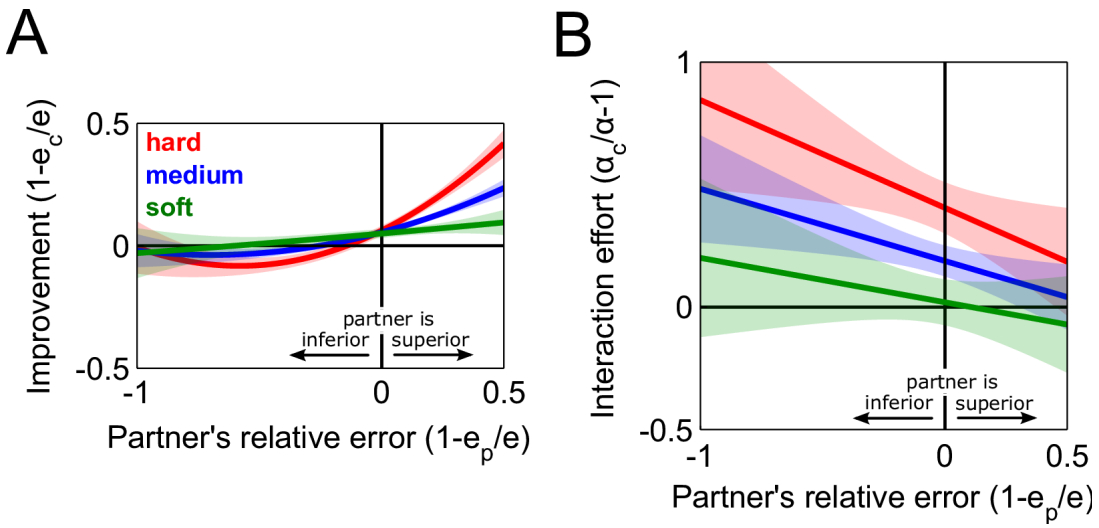

Figure 1-2: **Physical interaction between humans through different coupling dynamics (from [15])**. (A) Improvement, defined as the tracking error in a solo trial minus the error in the preceding connected trial, as a function of the relative error, defined as the difference in tracking errors between the partners in the solo trial. The improvement was modulated as a function of the coupling stiffness such that the worse partner (positive in the horizontal axis) improved more with the hard than with the soft interaction. However, the hard interaction did not hinder the better partner's performance. (B) Interaction effort, defined as the effort expended during a solo trial minus the effort in the preceding connected trial, as a function of the relative error. The effort was estimated as the sum of the mean muscle activations, normalised with respect to torque, from a wrist flexor and extensor pair. As with the improvement, the interaction effort is modulated by the softness of the interaction. Only the better partner in the hard and medium interactions exerted more effort in comparison to solo trials.

Perception is not a process taking only place at brain level, but can be counter-intuitively seen as a skillful activity of the system as a whole [22]: *active perception* is rather a problem of an intelligent data acquisition process where percepts do not simply fall onto sensors. For example, our pupils change size depending on the available light for increasing visual acuity [23]. The perception capabilities of the sensorimotor system is not solely the consequence of the control provided by the CNS. It is also affected by the system morphology (shape, position and type of sensors and effectors), by the material properties characterising its morphological components and by the physical constraints shaping its interactions with the environment [24]. The concurrent exploitation of sensorimotor interaction and body morphology produces statistical regularities in sensory inputs so that the information flow between sensors and effectors and the resulting perception is

actively shaped by the interaction dynamics [25]. This suggests that motor control can be understood as fulfilling prior expectations about proprioceptive, kinesthetic and tactile sensations [26]. Would it be possible to reshape and eventually improve human haptic sensing and the resulting perception by adjusting the body morphology or its material properties?

While the body anatomy cannot be changed, there is ample evidence that the CNS selectively controls the limb's viscoelasticity in response to instability and signal-dependent noise [27]–[31] to reduce kinematic variability by selective muscle activation [32], [33]. Recent studies examined how impedance influences sensing, suggesting the possibility to improve measurement through optimal impedance tuning [34]. In the case of free surface exploration, the adjustment of internal stiffness is further suspected to enhance haptic perception by regulating the function of mechanoreceptors and proprioceptive sensors such as tendon and spindle sensors located in muscles [35].

Given experimental evidence that is possible to influence the measurements accuracy by changing impedance, this research aims at testing if, and understand how, humans can modulate their limb viscoelasticity for obtaining reliable information and improving their visuo-haptic sensing.

Chapter 2 The nervous system can improve the visuo-haptic perception by optimising muscle cocontraction

---

Summary

While the nervous system can modify the body's stiffness by selective cocontraction to shape the mechanical interaction with the environment, little is known of how this influences haptic perception. Here, we show for the first time that the central nervous system can voluntarily adapt muscle cocontraction to increase haptic sensitivity. Subjects tracked a randomly moving noisy visual target while being physically guided by a virtual elastic band whose strength was controlled by the subject's cocontraction. They learned to increase cocontraction under visual noise and decreased it when the guidance was incongruent. Computational modelling revealed the adaptation law governing the CNS' regulation of the body's stiffness, which maximizes visuo-haptic information while minimising metabolic cost, trading off sensory information with energy.

Contribution Statement

The content of Chapter 2 has been developed by Gerolamo Carboni, with the contribution of Xiaoxiao Cheng, Thrishantha Nanayakkara, Atsushi Takagi and Etienne Burdet.
The contributions are as follows:

- GC carried out the experiment.

- GC, AT, performed the data analysis.
- GC, XC, AT, EB developed the statistical and computational modeling.
- GC, XC, TN, AT, EB have edited the text and agree with its content.

Some of this chapter's content has been published on *Scientific Reports* as: Carboni, G., Nanayakkara, T., Takagi, A. et al. Adapting the visuo-haptic perception through muscle coactivation. Sci Rep 11, 21986 (2021). https://doi.org/10.1038/s41598-021-01344-w.

2.1 Introduction

Humans are endowed with various sensors to interact with the environment, where haptics (the synthesis of touch and proprioception [2]) enables us to interpret physical interactions. In walking down a dimly lit flight of curved steps we instinctively reach out the handrail, that will guide our movement by providing haptic information about the steps direction. The guidance provided by the handrail becomes stronger when the arm is stiffened through muscle cocontraction [27], but how the body stiffness influences the haptic percept is unclear.

Could the central nervous system (CNS) modify haptic sensitivity by cocontracting muscles? The possibility and details of a mechanism driving such adaptive sensing have yet to be addressed. Haptics is challenging to investigate as the percept (the interaction force) is entwined with the mechanical guidance. Here, we disentangle the mechanical guidance from the haptic percept to study the brain's capacity to regulate its haptic sensitivity, and uncover the mechanism behind its regulation.

To this end, we developed a new paradigm wherein subjects used the cocontraction of a flexor-extensor pair of wrist muscle to control the strength of the elastic guidance while tracking a randomly moving target trajectory (Fig. 2-1A). An additional experiment was devised to isolate the mechanical effect of the elastic guidance, enabling us to study how the haptic percept changed with the wrist's stiffness. Using this paradigm, we

could systematically investigate whether and how the CNS adapts the body's stiffness in response to visual and haptic noise.

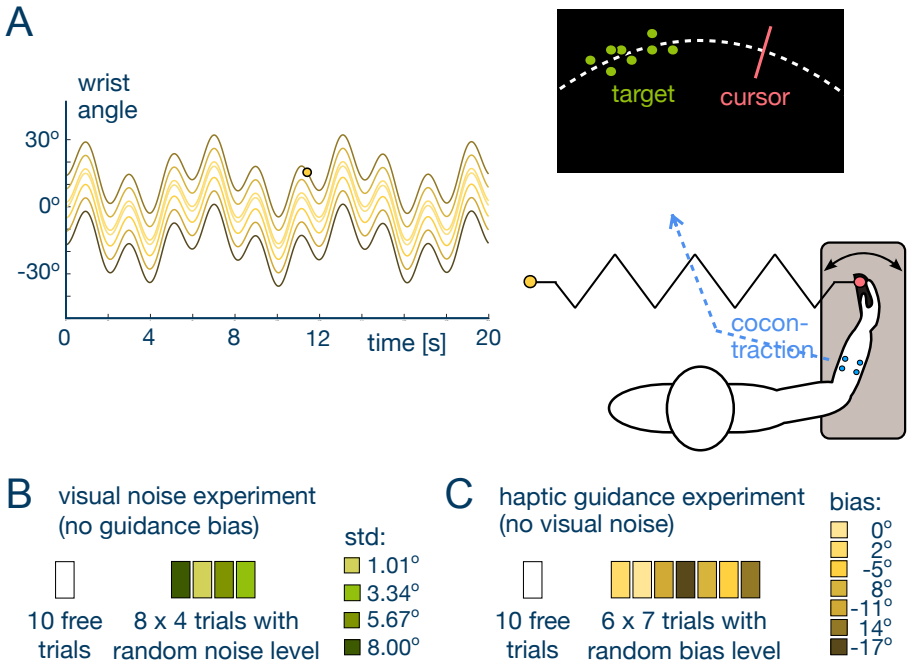

Figure 2-1: **Schematic of the experimental task and protocol.** (A) Subjects tracked a randomly moving target with their wrist flexion-extension movement while being guided by a virtual elastic band. The strength of the guidance increased with the cocontraction of a flexor-extensor muscle pair estimated from their myoelectrical activity. (B) Protocol of the experiment to study the effect of visual noise on the cocontraction. (C) Protocol to examine the effect of bias in the guidance trajectory with respect to the target on the cocontraction.

2.2 Methods

2.2.1 Subjects and experimental setup

The experiments described below were approved by the Joint Research Compliance Office at Imperial College London. A total of 59 subjects without known sensorimotor impairments, aged 21–36 years, including 22 females, were recruited to take part in one of the three main experiments and in the two experiments to identify the individual influence of haptics and vision. Each subject gave written informed consent prior to participation. The majority of subjects (56/59) were right-handed, as was assessed using the Edinburgh Handedness Inventory [36].

Each subject was seated comfortably on a height-adjustable chair next to the Hi5 robotic interface. The system consists of two 1 DoF flexion/extension wrist interfaces where the subject can lean the arm and easily hold a handle. This unique bilateral manipulandum-to-manipulandum system allows the subject to exchange interaction torques through the handle with both another human subject or a robotic controller. Subjects carried out the experiment individually and each of them held a single handle of the Hi5 dual robot with the dominant wrist as shown in Fig. 2-1A (further details on the Hi5 dual robotic interface can be found in [37]). This experimental setup has been selected not because considering the wrist joint activity the most relevant for haptics (for example, over the intrinsic hand muscles), but so that subjects could perform the experiments primarily activating a single flexor/extensor muscle pair with the aim of enhancing data clarity by reducing the complexity of the interaction dynamics. Along the line, subjects were also instructed to avoid fingers motion when pushing/pulling the handle. A screen placed in front of the subject provided visual feedback of the task with a cursor indicating the current wrist position (Fig. 2-1A). The Hi5 handle is connected to a current-controlled DC motor (MSS8, Mavilor) that can exert torques of up to 15 Nm, and was equipped with a differential encoder (RI 58-O, Hengstler) to measure the wrist angle and a force sensor (TRT-100, Transducer Technologies) to measure the exerted torque in the range [0,11.29] Nm. The Hi5 system is controlled at 1kHz using Labview Real-Time v14.0 (National Instruments) and a data acquisition board (DAQ-PCI-6221, National Instruments), while data was recorded at 100 Hz.

The activation of two antagonist wrist muscles, the flexor carpi radialis (FCR) and extensor carpi radialis longus (ECRL), were recorded with surface electrodes using a medically certified non-invasive electromyography system (g.LADYBird + g.GAMMABox + g.BSamp, g.Tec). The raw muscle activity was high-pass filtered at 20 Hz, rectified, then low-pass filtered at 5 Hz. The filtering process yielding the filtered muscle activity was in both cases a second-order Butterworth filter.

2.2.2 Muscle activation calibration and cocontraction computation

Every experiment started with an *EMG normalization* to map the raw muscle activity (in mV) to a corresponding torque value (in Nm). The subject placed their wrist in the most comfortable middle posture, which was set to 0°. Constrained at that posture, they were then instructed to sequentially (*i*) flex, or extend the wrist to exert a torque, or (*ii*) maximally co-contract in order to keep the wrist position stable during a 3 Hz sinusoidal positional disturbance of 10° amplitude. Each phase was 4 s long with a 5 s rest period between consecutive contraction phases to avoid fatigue, which was used as a reference activity in the relaxed condition. This was repeated four times at flexion/extension torque levels {1,2,3,4} Nm and {-1,-2,-3,-4} Nm, respectively. For each subject, the recorded muscle activity was linearly regressed against the torque values to estimate the relationship between them. Therefore, the torque associated with the flexor muscle was modelled from the filtered EMG signal depicting the flexor muscle activation u_f as

$$\tau_f(t) = \alpha_0 u_f(t) + \alpha_1, \quad \alpha_0, \alpha_1 > 0, \tag{2.1}$$

and similarly for the torque of the extensor muscle τ_e. The variables α_0, α_1 computed from the linear regression for both flexion and extension are subject specific. *Muscle cocontraction* was then computed as

$$u(t) \equiv \min\{\tau_f(t), \tau_e(t)\}. \tag{2.2}$$

The muscle cocontraction $u(t)$ represents an indicator of joint stiffening that stems from contracting a pair of antagonist muscles. This cocontraction indicator does not take into account the absolute activation of a single muscle and the resulting change of stiffness if the other muscle does not change its activity. The average cocontraction over all subjects (as shown in Figs. 2-3B,D) was computed from each subject's normalised cocontraction,

calculated as

$$u_n \equiv \frac{\overline{u} - \overline{u}_{min}}{\overline{u}_{max} - \overline{u}_{min}}, \quad \overline{u} \equiv \frac{1}{T}\int_0^T u(t)\,dt, \quad T = 20\,s \tag{2.3}$$

with $\overline{u}_{min}$ and $\overline{u}_{max}$ the minimum and maximum of the means of all trials for the specific subject.

2.2.3 Tracking with visual and haptic feedback

In the three main experiments of sections 2.2.4 - 2.2.6, subjects were required to track a *visual target* (in degrees) moving with

$$q^*(t) \equiv 18.5 \sin\left(\frac{\pi t^*}{1.547}\right) \sin\left(\frac{\pi t^*}{2.875}\right), \quad t^* \equiv t + t_0\,, \quad 0 \le t \le 20\,s \tag{2.4}$$

using flexion-extension movements (Fig. 2-1A). To avoid trajectory memorisation, t^* started in each trial from a randomly selected zero $\{t_0 \in [0,20]\,\mathrm{s} \mid q^*(t_0) \equiv 0\}$ of the multi-sine function. After each 20 s long trial, the target disappeared and the subject was required to place the hand on the starting position at the center of the screen. The next trial then started after a 5 s rest period and a 3 s countdown. Each subject was instructed to take small breaks when feeling (mental or physical) fatigue during the course of the experiment. The *tracking error*

$$e \equiv \left(\frac{1}{T}\int_0^T [q^*(t) - q(t)]^2\,dt\right)^{\frac{1}{2}}, \; T \equiv 20\,s \tag{2.5}$$

was displayed at the end of each trial, where $q(t)$ is the wrist angle.

The tracking task consisted of a *free phase* (in which no interaction torque was exerted on the wrist) to get the subject accustomed with the Hi5 interface, followed by an *interaction phase* in which the subject's wrist position was connected to a *haptic reference trajectory* $q_h(t)$ with an elastic force

$$\tau(t) = \kappa(t)\,[q_h(t) - q(t)], \quad \kappa(t) \equiv \frac{u(t)}{8} \tag{2.6}$$

where the connection stiffness $\kappa < 0.25\,\mathrm{Nm}/^\circ$ linearly increased with the cocontraction $u(t)$.

Subjects were informed of the possibility to regulate the coupling stiffness by co-contracting or relaxing wrist's muscles, and of the transition between free trials and interaction trials. They were further instructed not to resist large torques provided by the motor.

2.2.4 Visual noise experiment

In this experiment $q_h \equiv q^*$ thus there was no haptic noise. A visual noise experiment was carried out by 15 right-handed subjects (7 females, aged 23.46±2.39 years old). The target trajectory was displayed on the screen either as a 8 mm diameter circle or as a "cloud" of eight normally distributed dots around the target (Fig. 2-1A), depending on the experimental condition. The cloud of dots were defined by three parameters, randomly picked from independent Gaussian distributions: the vertical distance to the target position $\eta \in \mathrm{N}(0, 15\,\mathrm{mm})$, the angular distance to the target position $\eta_q \in \mathrm{N}(0, 1.01^\circ < \sigma_v < 8.00^\circ)$, and the angular velocity $\eta_{\dot{q}} \in \mathrm{N}(0, 4^\circ/\mathrm{s})$. The amplitude of visual noise was controlled by the angular distance deviation, while both the vertical and the angular velocity deviations were kept constant. The dots were updated sequentially so that each dot was replaced every 100 ms. The experimental protocol consisted of 10 free trials followed by 32 interaction trials split into 8 blocks. The 4 trials of each block used a different value of $\sigma_v \in \{1.01^\circ, 3.34^\circ, 5.67^\circ, 8.00^\circ\}$ presented in a random order in each block (Fig. 2-1B). We assume that the ordering of the blocks has no effect.

2.2.5 Haptic bias experiment

In this experiment the target was a 8 cm diameter disk, and the elastic guidance trajectory was biased by δ relative to the target trajectory:

$$q_h(t) = q^*(t) + \delta\,. \tag{2.7}$$

Another 13 subjects (4 females, 12 right-handed, aged 23.53±3.03 years old), carried out a haptic noise experiment. The experiment consisted of 52 trials with 10 free trials followed by 42 interaction trials subdivided into 6 blocks. The 7 trials of each block had a different $\delta \in \{0^\circ, 2^\circ, -5^\circ, 8^\circ, -11^\circ, 14^\circ, -17^\circ\}$, where these bias conditions were presented in a random order in each block (Fig. 2-1C). We assume that the ordering of the blocks has no effect.

2.2.6 Visual noise and haptic bias experiment

A third experiment with both visual noise and haptic bias was carried out with 15 subjects (aged 25.06±2.12 years old, with 5 females, 14 right-handed). The protocol consisted of 40 trials with 8 free trials, followed by a 32 interaction trials in 8 blocks of 4 trials. In these 4 trials, the subject experienced different combinations of the guidance bias and visual noise $(\delta, \sigma_v) \in \{(1.5^\circ, 0^\circ), (1.5^\circ, 6.7^\circ), (8.5^\circ, 0^\circ), (8.5^\circ, 6.7^\circ)\}$, presented in a random order in each block.

2.2.7 Haptic noise model

Haptic noise relative to the target movement is due to the biased reference trajectory relative to the target (resulting in the movement standard deviation σ_b relative to the target trajectory) and to the elasticity of the virtual band [15]. Assuming that these effects are independent and that the band elasticity results in zero mean noise with deviation $\sigma_\kappa(u)$, the haptic noise deviation can be calculated as

$$\sigma_h^2(u) = \sigma_b^2 + \sigma_\kappa^2(u)\,. \tag{2.8}$$

The effect of the reference trajectory bias is described through

$$\sigma_b = \alpha_b + \delta^\theta \tag{2.9}$$

with subject specific $\alpha_b, \theta > 0$. Two additional experiments were carried out to observe the tracking performance as either a function of the visual noise or as a function of the virtual band's elasticity in order to specify the haptic noise.

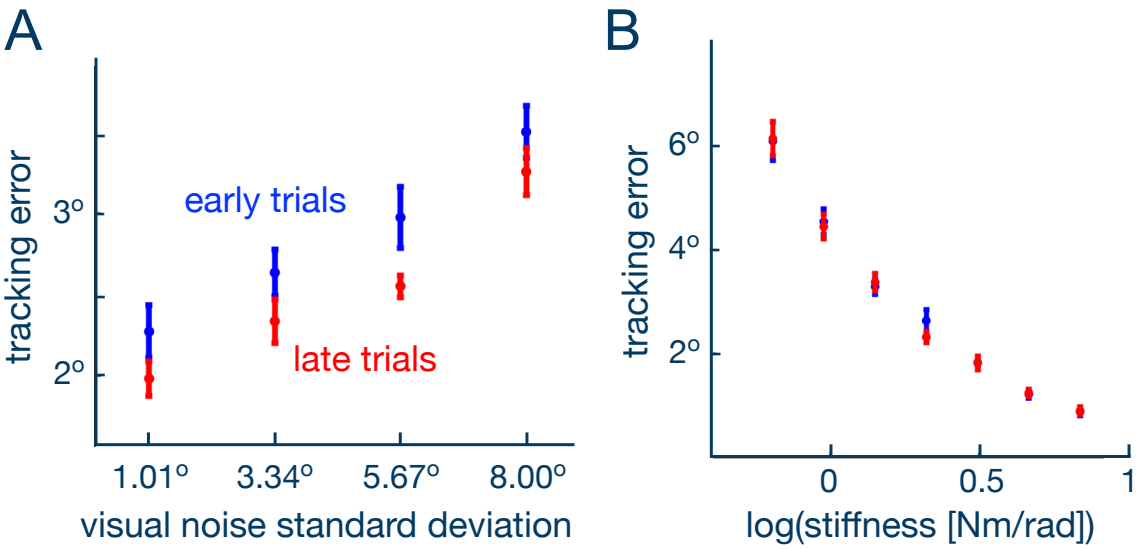

Figure 2-2: Results of experiments to isolate the effect of visual feedback and haptic guidance on the tracking performance. (A) In the visual noise experiment, the tracking error linearly grew with visual noise, and decreased across all noise levels after learning. (B) In the experiment with haptic feedback only, the tracking error decreased with the log of the elasticity (linear mixed-effect analysis, $p<0.001$). This relationship did not change with practice.

A *visual experiment* was carried out to evaluate the influence of the visual noise on the tracking performance. No elastic force was present in this experiment. Eight right-handed subjects not involved in the main experiments (25.01 ± 0.53 years old, including 2 females) participated in this study. The protocol was similar to the main experiments, consisting of 42 trials divided in initial trials for task familiarisation and a following testing phase. Each trial lasted 20 seconds. In the acclimatisation phase, consisting of 10 trials without visual noise, the target's position was displayed by a single point. In the remaining 32 trials of the testing phase, the trials were organized into 8 blocks, each containing 4 trials with visual noise $\sigma_v \in \{1.01°, 3.34°, 5.67°, 8.00°\}$. The four levels of visual noise were randomized in each block. The results show that the tracking error is linearly correlated with the visual noise imposed on the target (Fig. 2-2A, [38]).

This was modelled as

$$e_v(\sigma_v) = \alpha_v + \beta_v \sigma_v , \tag{2.10}$$

$\alpha_v = -11.67, \beta_v = 0.13$ were identified from a least-squares linear regression with data from late trials.

Next, a *haptic experiment* was performed to measure how the tracking error depended on the elasticity of the virtual band. In this experiment, no visual feedback was provided while the wrist was connected to the target reference trajectory with 7 selected levels of elasticity. Another eight subjects (7/8 right-handed, 26.75±1.28 years old, including 4 females) participated in this experiment. The experiment was structured in 5 blocks of 7 elasticity values $\kappa \in \{0.011, 0.016, 0.025, 0.037, 0.055, 0.081, 0.120\}$ Nm/° presented in random order. In the 35 interaction trials, the subjects experienced an elastic force to the target. As expected, the tracking error decreased with increasing elasticity (Fig. 2-2B), which was modelled as an exponential function

$$e_h(\kappa) = \alpha_h e^{-\beta_h \kappa} + \gamma_h , \tag{2.11}$$

where $\alpha_h = 4.42$, $\beta_h = -7.59$, $\gamma_h = 4.15$ were identified from a least-square fit.

To compare the deviations of tracking error due to visual and haptic noise, the error due to haptic noise was transformed to its equivalent value in visual noise. This was carried out by setting $e(\kappa) \equiv e(\sigma_v)$, yielding

$$\sigma_\kappa(u) = \xi_0 + \xi_1 e^{-\beta_\kappa u}, \quad \xi_0 \equiv (\gamma_h - \alpha_v)/\beta_v , \quad \xi_1 \equiv \alpha_h/\beta_v , \quad \beta_\kappa \equiv \beta_h/8 \tag{2.12}$$

2.2.8 Statistical integration

To statistically model the adaptation mechanism, the visual error e_v was generated from a Gaussian distribution (with $\sigma_v \in \{1.01°,\ 3.34°,$
$5.67°,\ 8.00°\}$) around the average error in the last two blocks of the visual control

experiment (see Fig. 2-2A). To estimate the haptic error e_h, the mean stiffness values recorded over the last two experimental blocks of the *visual and haptic bias experiment* (section 2.2.6) was first computed. Then, this averaged coupling value was given as input to calculate e_h from the square fit of the data in the haptic control experiment (Fig. 2-2B). The standard deviation $\sigma_h(u)$, necessary to compute the weights in the Bayesian integration model introduced in equation 2.18, was obtained from e_h by inverting the mapping obtained to fit the visual control experiment in a similar fashion to eq. 2.12.

2.2.9 Haptic noise experiment simulation

Tracking error minimization (TEM)

For each of the 7 bias levels $\{i\}$, the initial coactivation level $\{\hat{u}_i(1)\}$ was first set as the initial experimental value $\{u_i(1)\}$. Then, by using the respective trial-by-trial tracking error $\{e_i(k)\}, k = 1, ..., 5$ from the experiment, the adaptation parameters α, γ in the computational model of eq.(2.19) were computed to minimize the error between the learned values after 5 iterations $\{\hat{u}_i(6)\}$ and the corresponding data $\{u_i(6)\}$ in last experiment's trial:

$$(\alpha^*, \gamma^*) \equiv \underset{\alpha,\gamma>0}{\arg\min} \left\{ \sum_{i=1}^{7} \left[\hat{u}_i(6) - u_i(6)\right]^2 \right\}. \tag{2.13}$$

The parameters $\alpha^* \equiv 0.01, \gamma^* \equiv 0.14$ were found by using a grid search with a step 0.01 in the range $[0,2] \times [0,2]$.

Optimal information and effort (OIE)

A gradient descent optimisation is used to minimize the prediction error and effort in eq.(2.21). Muscle cocontraction is updated trial after trial using:

$$\begin{aligned} u_{new} &= u - \frac{dV(u)}{du} = -\frac{dE(u)}{du} + (1-\gamma)\,u\,, \\ -\frac{dE(u)}{du} &= \left[\frac{\sigma_v^2}{\sigma_h^2 + \sigma_v^2}\right]^2 \left[-\frac{d\sigma_h^2(u)}{du}\right] > 0\,. \end{aligned} \tag{2.14}$$

where γ, α_b and θ were computed by minimizing the variation of the cost derivative:

$$(\gamma^*, \theta^*, \alpha_b^*) \equiv \underset{\gamma,\theta,\alpha_b>0}{\arg\min} \left\{ \sum_{i=1}^{7} \left[\frac{dV}{du} \left[\hat{u}_i(6),\, \sigma_{h,i}(\alpha_b, \theta),\, \sigma_{v,i} \right] \right]^2 \right\} \tag{2.15}$$

Assuming $\sigma_v \equiv 2$ for the minimal visual noise standard deviation and using the learned cocontraction data $\{u_i(6)\}$, $\gamma^* = 0.106$, $\theta^* = 2.5$, $\alpha_b^* = 30$ determined through a grid search for (θ, α_b) in $[0,3] \times [0,40]$ with steps 0.5 and 1 respectively, where for each gridpoint γ was the solution to

$$0 \equiv \frac{d}{d\gamma} \left[\sum_{i=1}^{7} \left(\frac{dV_i}{du} \right)^2 \right]. \tag{2.16}$$

Bayesian error minimization (BEM)

BEM was considered as a special case of OIE model with $\gamma \approx 0$. $\theta^* = 3$, $\alpha_b^* = 40$ were determined by using the same grid search as above with $\gamma \equiv 10^{-5}$.

2.3 Experimental results

We first examined the results from a *visual noise tracking experiment* wherein increasing amounts of visual noise were imposed on the target to which the subjects were elastically guided (Fig. 2-1B). The strength of the elastic guidance was controlled by the subjects themselves through the cocontraction of their wrist. Figs. 2-3A and 2-3B show the square root of square error over a trial or *tracking error* (defined in the Methods through eq.(2.5)) and the mean *cocontraction* as a function of the block number, separately for each level of visual noise.

The tracking error magnitude was large but gradually decreased over blocks (Fig. 2-3A). The effect of training was measured by comparing the error in the first and last blocks. A two-way repeated measures ANOVA (RANOVA) showed that both the visual noise ($p<0.001$, $F(3,40)=8.67$) and the training ($p=0.002$, $F(1,12)=14.34$) had a significant influence on the error. Post-hoc comparisons using Tukey's Honest Significant Difference

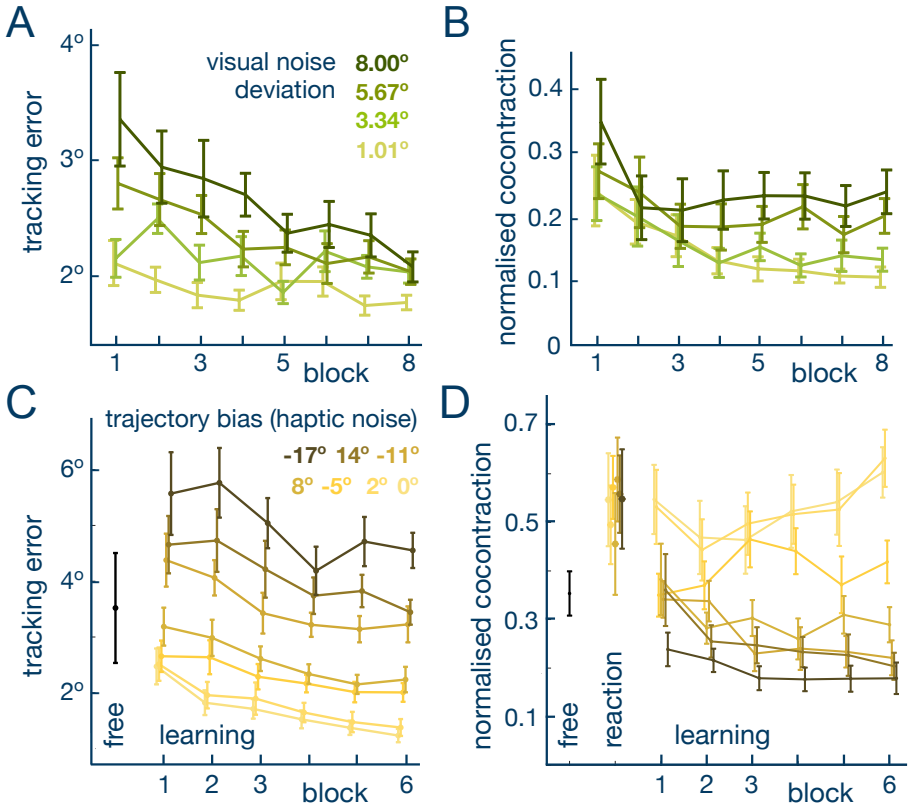

Figure 2-3: **Tracking error and muscle cocontraction.** Adaptation with training in both the *visual noise tracking experiment* (A,B) and *haptic bias experiment* (C,D). The figures show the mean values with standard error bar over all subjects of each trial in the corresponding block. (A) The population mean tracking error and the associated variability decreased with trials for every level of visual noise. (B) The normalised cocontraction was initially large in the first block of trials for all visual noise conditions and decreased with practise. The level to which the cocontraction converged was dependent on the visual noise imposed on the target. (C) In the haptic bias experiment the tracking error magnitude over one trial decreased with training, with higher error when the haptic bias was greater. (D) The initial cocontraction was comparable for all haptic bias levels, but subjects gradually learned to increase the elastic stiffness with smaller haptic bias and decrease it with large haptic bias.

criterion (HSD) confirmed a decrease of tracking error with training for the two higher levels of visual noise ($p=0.027$ and $p<0.001$ respectively).

We then looked at how the mean cocontraction measured over a whole trial depended on the visual noise and the block number. The cocontraction was normalized for comparisons between subjects. Another two-way RANOVA revealed a significant effect of both the visual noise level ($p<0.001$, $F(3,40)=8.3$) and training ($p=0.01$, $F(1,12)=8.9$) on the normalized cocontraction. Post-hoc comparisons confirmed that the normalized cocontraction

in the first block was comparable across all visual noise levels, but different between the lowest and highest visual noise levels in the last block ($p=0.02$). The normalized cocontraction tended to decrease over blocks by a larger amount when the visual noise was lower. This yielded a normalized cocontraction in the final three blocks that increased monotonically with the level of visual noise (slope=0.0185 ± 0.002, one-sample t-test $t(2)=13.15$, $p<0.006$). This suggests that the CNS adapts the body's stiffness to modify the haptic guidance in response to visual noise on the target.

To test whether haptic sensitivity is adapted in response to the quality of the haptic information arising from the guidance, we examined the results from a *haptic bias tracking experiment* where the target was displayed without visual noise but the guidance trajectory was shifted from the target by increasing amounts, from henceforth referred to as *guidance bias* (Figs. 2-1A,C). The tracking error tended to increase with the magnitude of the guidance bias as shown in Fig. 2-3C. A two-way RANOVA highlighted the influence of the guidance bias ($p<0.001$, $F(6,71)=28.44$) and the training ($p<0.001$, $F(1,12)=18.96$) on the tracking error. Post-hoc comparisons revealed a significant decline in the error between the first and the last blocks across all bias levels. The error was also higher with greater bias ($p<0.001$ comparing highest and lowest bias).

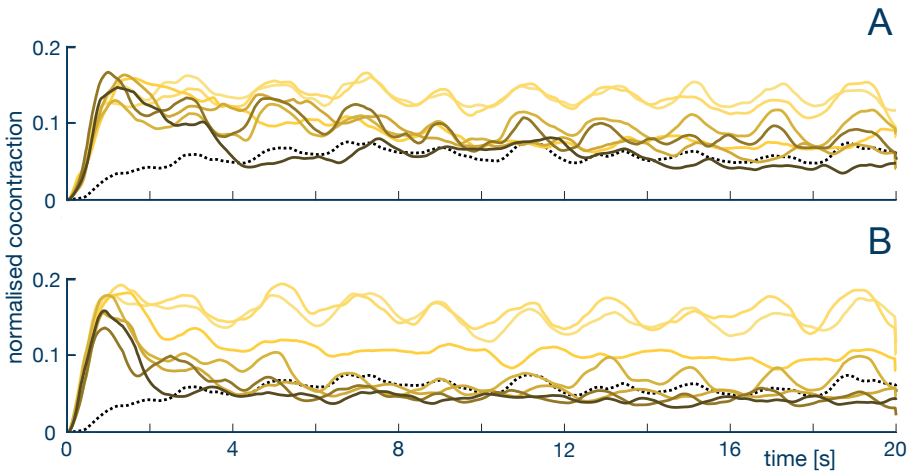

Figure 2-4: **Evolution of normalised cocontraction when tracking with haptic bias.** Cocontraction waveforms with different trajectory bias in the first (A) and last (B) blocks. The data exhibits quicker settlement to discrete and stable levels of coactivation for different trajectory biases in last block (2 s vs. 4 s).

The improvement in the tracking error with guidance bias was also accompanied by an adaptation of the wrist's cocontraction (Fig. 2-3D). We first analyzed how the subjects reacted to the different levels of bias by measuring the mean normalized cocontraction in the first 200 ms (see Figs. 2-3D, 2-4). Subjects initially reacted to the guidance by cocontracting greatly regardless of the bias ($p=0.78$, $F(6,71)=0.44$, repeated measures ANOVA on the different bias level conditions with Greenhouse-Geisser correction). However, the normalized cocontraction tended to decrease thereafter on trials with a large bias, and increased on select trials wherein the bias was small, as if the CNS was modulating the cocontraction in response to the congruency between the target and the guidance. A one-way RANOVA confirmed that larger bias was associated with smaller cocontraction in the last block ($p<0.001$, $F(1,12)=153.09$). It appears that the CNS also modulated the body's stiffness in response to the quality of the haptic guidance.

The subjects in both the visual noise and the guidance experiments improved their tracking performance with training, and modified the body's stiffness depending on the level of the visual noise and the amount of bias on the guidance trajectory. Increasing visual noise induced subjects to increase their cocontraction, in line with previous studies on learning in unpredictable dynamic environments [29], [39]. However, large haptic noise caused a reduction in the cocontraction, in contrast to the effect observed in unpredictable dynamic environments [29], [39]. The CNS had seemingly learned to modify the body's stiffness in accordance with its effect on the tracking performance.

2.4 Statistical modelling

While learning is known to be generally accompanied by a decrease of muscle cocontraction [30], [40], this would not explain the distinct cocontraction levels observed at the end of the learning phase for the different visual noise conditions. Why did subjects increase cocontraction as a function of visual noise?

To address this question, we analyzed how the sensory information of the target's motion from vision and haptics was combined by the NS. We considered the tracking performance as a linear function of the amount of visual error e_v and haptic error e_h:

$$e \equiv w_h e_v + w_v e_h, \quad w_h, w_v > 0, \tag{2.17}$$

and tested four models expressing different combinations of the visual and haptic information. The *visual dependence model* expresses that only information of the target's motion from vision is used to track the target, such that the performance is fully explained by the reliability of vision alone (w_h=1, w_v=0). The *haptic dependence model* expresses the converse, where haptic information alone is used to track the target (w_h=0, w_v=1). In the *averaging model*, visual and haptic information are weighted equally to track the target ($w_h = w_v = 1/2$). The *Bayesian integration model* assumes that a stochastically optimal weighted average is used to minimize the prediction error considering information from vision and haptic sensing:

$$w_h = \frac{\sigma_h^2}{\sigma_v^2 + \sigma_h^2}, \quad w_v = \frac{\sigma_v^2}{\sigma_v^2 + \sigma_h^2} \tag{2.18}$$

with σ_v and σ_h the standard deviations of visual and haptic noise, respectively. Each model yielded a different prediction of the task performance for a given visual noise level and cocontraction value. By comparing the predicted task error and the empirically measured error, we could assess which model best explained the sensory combination of vision and haptics.

We first analyzed how each model's predicted performance depended on the visual noise condition (Fig. 2-5A). Unsurprisingly, the visual dependence model predicted greater error as visual noise increased. Conversely, the haptic dependence model predicted decreasing error with visual noise since the cocontraction was greater with higher visual noise. The averaging model predicted a roughly constant error irrespective of the visual noise value.

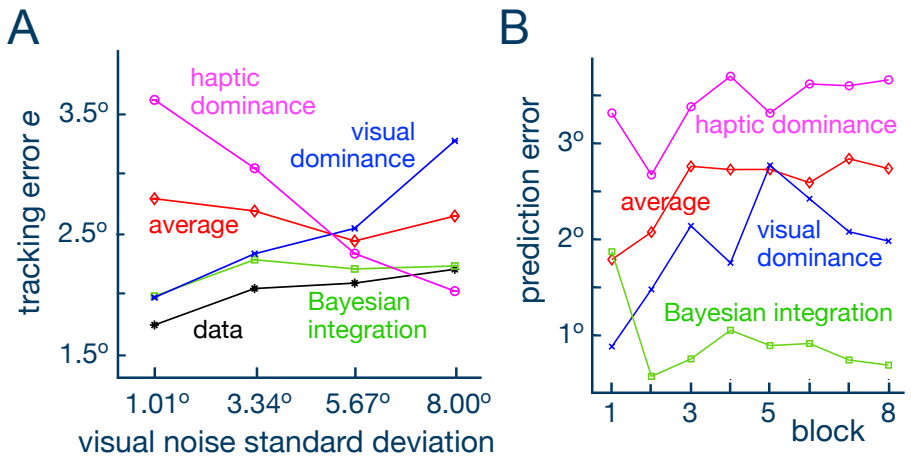

Figure 2-5: **Statistical modelling.** The best model that minimised the prediction error was the Bayesian integration of visual and haptic information. (A) The tracking performances predicted by each model for the last block are plotted as a function of the visual noise. With the increase of visual noise, the *visual dependence* model diverged from the experimental data. In contrast, the *haptic dependence* model predicted large error with low visual noise, which was different from the data. The error predicted by the *Bayesian integration* model was closest to the empirical data for all levels of visual noise. (B) The predicted error from each model is plotted as a function of the block number. In the first block, the *visual dependence* model yielded the lowest prediction error. From the second block onwards, the *Bayesian integration* model outperformed the others, with both the *visual dependence* and the *averaging* models' predictions inflating with trials. The *haptic dependence* mode yielded the worst prediction.

The predicted performance from the Bayesian integration model was the nearest to the empirical data. A two-way repeated measure ANOVA of the difference between the model and experimental data revealed a significant influence of the different models on the estimation ($p<0.001$, $F(3,56)=5.75$), while the effect of visual noise level had a negligible effect. Post-hoc comparisons both confirmed the similarity of the Bayesian integration model predicted with experimental data ($p>0.1$), and their difference to predictions from the other models ($p<0.001$).

We then examined how the prediction error (computed as the maximum likelihood estimate of the difference between the task error predicted by each model and the empirical error from the experimental data) changed as a function of the trials' blocks. The visual dependence model yielded the smallest prediction error in the first block (Fig. 2-5B). However, its prediction faltered in later blocks. The haptic dependence model yielded

the worst prediction of all four models, with the prediction error growing in later blocks. The averaging model laid in between the visual and haptic dependence models, which indicates that the information from the two sensory channels was not weighted equally by the NS. The Bayesian integration model was the best model in all blocks but the first. This suggests that subjects may have relied mainly on vision in the first block to track the target, but gradually learned to integrate haptic percepts from the second block onwards to improve performance.

2.5 Computational adaptation mechanism

The improvements in the tracking performance could be purely due to the mechanical effect of the guidance. To test this possibility, we simulated a computational model according to which cocontraction is modulated to minimize the tracking error, which explains its adaptation when interacting with various dynamic environments [41]. In this model, the cocontraction increases with the tracking error e and decreases with each new trial according to

$$u_{new} \equiv \alpha e + (1-\gamma) u\,, \quad \alpha, \gamma > 0\,. \tag{2.19}$$

Simulation of the visual noise experiment with this *tracking error minimization* (TEM) model predicted an increase in cocontraction with the visual noise, corresponding to the trend observed in the experimental data, albeit not capturing its variability (Fig. 2-6A). We then simulated its predictions for the guidance bias experiment. The model predicted an increase in the coactivation with the bias, opposite to what was observed in the experiment (Fig. 2-6B). While the TEM model could capture the change in the cocontraction as a function of visual noise, it cannot explain the results of the guidance bias experiment.

Alternatively, as suggested by our statistical modelling, the CNS may be actively modifying the body's stiffness to regulate its haptic sensitivity and use this information to improve motor performance. Since the cocontraction adapted to both visual noise and the guidance bias, it may be determined by the statistical information from vision and haptics, characterized

by their respective standard deviations σ_h and σ_v. Specifically, cocontraction could be adapted to minimize the Bayesian prediction error

$$E(u) \equiv \frac{\sigma_h^2(u)\,\sigma_v^2}{\sigma_h^2(u)+\sigma_v^2} \tag{2.20}$$

that depends on the cocontraction through $\sigma_h(u)$. Simulations with this *Bayesian error minimization* (BEM) model predict an increase in the cocontraction with greater visual noise (Fig. 2-6A) as well as smaller cocontraction with larger bias (Fig. 2-6B), corresponding to the tendencies observed in the experimental data. However, the cocontraction in the BEM model increases to values outside of the range observed in the experiments.

These results suggest that while the prediction error is considered by the CNS, the BEM model misses a fundamental mechanism to regulate the overall cocontraction level. Considering the natural tendency to minimize cocontraction during learning [40], [41], we propose that a function consisting of the prediction error and the metabolic cost

$$V(u) \equiv E(u) + \frac{\gamma}{2}u^2, \quad \gamma > 0 \tag{2.21}$$

is minimized. Simulations with this *optimal information and effort* (OIE) model exhibit an increase in the cocontraction with greater visual noise (Fig. 2-6A), as well as a decrease in the cocontraction with increasing guidance bias (Fig. 2-6B). Crucially, the OIE model's predicted normalized cocontraction corresponds accurately to those of the data with an error of 0.02 ± 0.01.

The OIE model further predicts how coactivation will be modulated in the presence of both visual noise and guidance bias (blue surface of Fig.2-6C). We tested the OIE predictive capability by conducting a third experiment where the visual noise and the guidance bias were concurrently manipulated across trials. An aligned ranks transformation ANOVA (ART ANOVA) with repeated measurements revealed that the normalized cocontraction was significantly influenced by the guidance bias ($p<0.001$, $F(1,98)=61.91$), weakly influenced

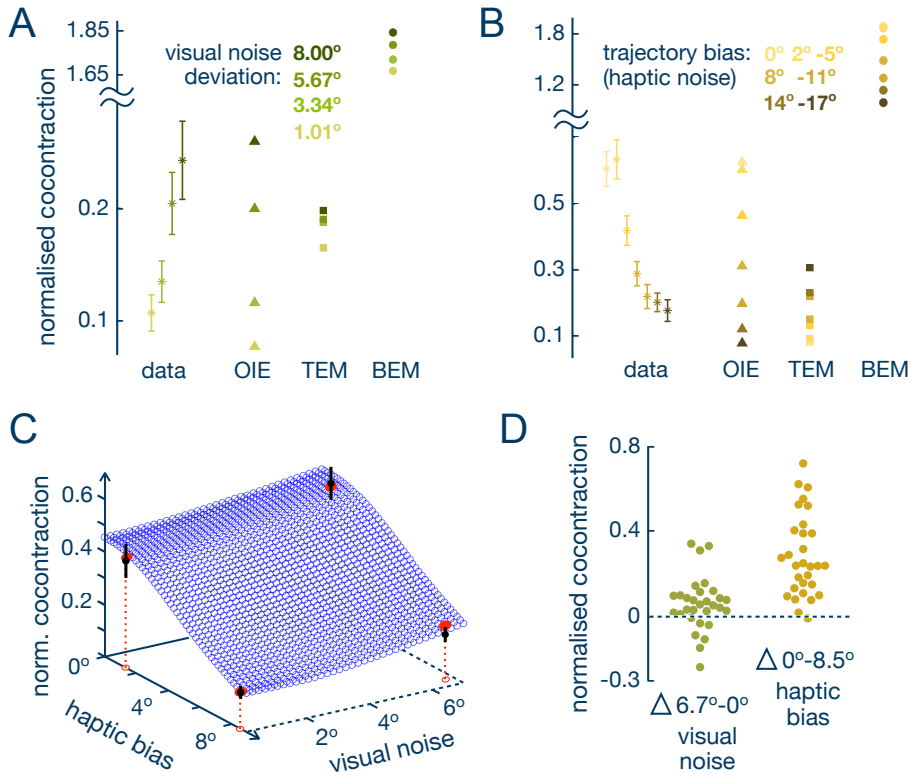

Figure 2-6: **Computational modeling of adaptation to visual and haptic perturbations.** (A) The cocontraction in the last block of the visual noise experiment is compared with the prediction of the *tracking error minimization* (TEM), *Bayesian error minimization* (BEM) and *optimal information and effort* (OIE) models. (B) The cocontraction in the last block of the guidance bias experiment is compared with the predictions from the above mentioned models. TEM showed the opposite trend to the data, the BEM exhibited a correct trend but with diverging values, while the results predicted by OIE resembled the data. (C) A third experiment with concurrent changes in visual noise and guidance bias was carried out. The protocol involved 8 blocks of 4 trials with bias and visual noise conditions corresponding to the red dots presented in random order. The corresponding mean values and standard error are shown in black. The OIE model (red dots on the surface) predicts an increase in cocontraction both as a function of the visual noise and the bias. (D) Corresponding difference of cocontraction with a larger visual noise standard deviation and smaller haptic guidance bias.

by the visual noise level ($p=0.14$, $F(1,98)=2.16$), and not affected by the training ($p=0.56$, $F(1,98)=0.35$) (Figs. 2-6D, 2-7). Post-hoc comparisons revealed how the normalized cocontraction increased with larger visual noise ($p=0.025$) and decreased with a larger haptic bias ($p<0.001$). The cocontraction in this third experiment was indeed modulated by both visual noise and bias as predicted by the OIE model (Fig. 2-6C), a testament to its predictive power.

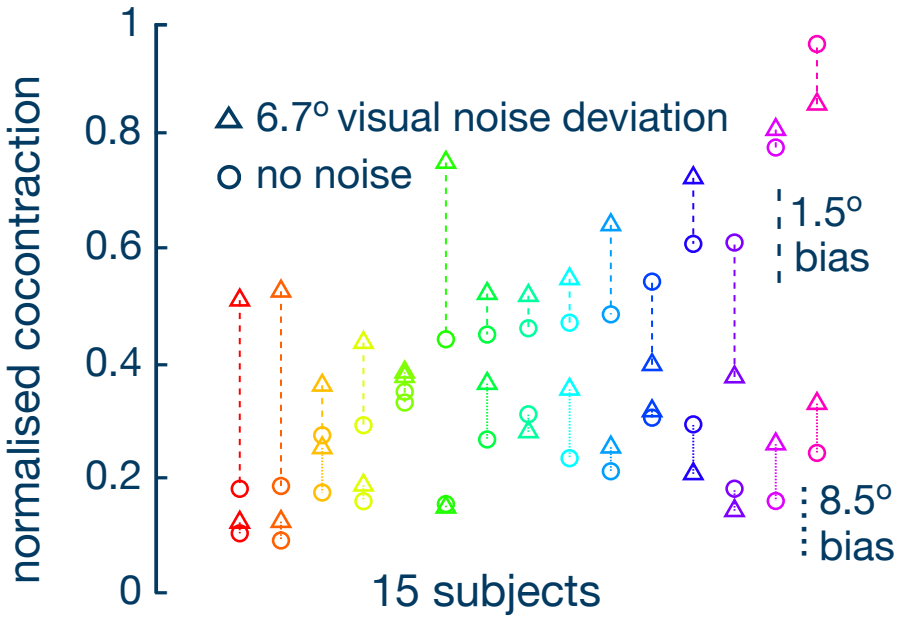

Figure 2-7: **Cocontraction modulation with visual noise and haptic bias.** For most of the 15 subjects taking part in the experiment with concurrent changes in visual noise and guidance bias, the cocontraction increased with visual noise while the larger haptic bias led to decreasing it.

2.6 Discussion

While haptic sensing is used to guide actions, here we show that the brain can take an action to improve haptic sensing of the environment. Our experimental results reveal that the brain activates muscle groups to modify the arm's compliance, making it stiffer when better haptic sensing could improve task performance. Past studies have shown how the CNS controls the body's stiffness to shape the mechanical interaction with the environment [29], [42], [43], and morphological computation has analysed how the biomechanical design in animals facilitates their functions [24], [44]. Different from these motor and morphological adaptations, our results provide the first evidence that the CNS can actively control the body's stiffness *to regulate its haptic sensitivity*.

The computational mechanism of adaptive sensing introduced in this chapter suggests that the brain tries to maximize information from vision and haptics while minimizing energetic costs. The association of sensory modalities and their stochastically optimal integration has been reported in numerous studies [16], [19], [20], whereby the reliability

of each sensory input was manipulated externally by the experimenter. In contrast, the haptic sensitivity in our experiment was actively controlled by the subjects themselves through the strength of the guidance.

While previous studies have provided qualitative evidence of humans spontaneously adapting their sensors' acuity to improve perception when undertaking physical interaction tasks [45]–[47], we could quantify the performance improvement resulting from the reduction in haptic noise as a consequence of greater body stiffness or cocontraction. Importantly, to obtain these results, it was necessary to subtract the mechanical guidance from the haptic percept. The haptic tracking control experiment enabled us to isolate the mechanical effect of the haptic guidance on the tracking performance, and then deduct it to determine how the haptic percept was influenced by the limb's cocontraction.

The optimisation of mechanical properties observed in our study may contribute to the performance benefits observed when physically connected pairs carry out a common task [48]. Cocontraction may be tuned to improve sensing of the partner's movement [15], thus enabling faster learning and improved assistance. The increase of visuo-haptic accuracy observed in our experiment may also explain why increasing the body's stiffness can speed up the acquisition of internal models of novel dynamics [49].

Recent models [50], [51] clarified how major characteristics of motor memory correspond to the minimisation of motor error and its history. These models however do not possess a mechanism to deal with muscle stiffness so cannot explain our results nor those from [29]. On the other hand, a range of experimental evidence from arm movements carried out in various spatial, temporal and dynamic conditions suggest that planned actions minimise task error and metabolic cost in the presence of motor noise [41], [52]–[54]. However, these studies did not consider sensory noise and its influence on the cost function. Our study provides evidence that the CNS also considers noise in the sensory signals and voluntarily controls the muscle activation to minimise task error and metabolic cost. The

CNS adapts the motor commands to improve visuo-haptic perception through an optimal trade-off of information and energy.

Chapter 3 Local adaptation of muscle activation to improve task performance

---

Summary

The information emerging from haptic interactions depends on the body features and is shaped by the perception-actuation loop. While it is recognised that the brain exploits the body dynamics to ease control and facilitate perception, it is not clear whether and how it would compensate when the body morphology and the muscle activation patterns are undermining performance in a given task. In this chapter, we investigate the human capability of thoughtfully modulating body properties to deal with the haptic information originating from physical interaction. A continuous tracking experiment in which the subjects motion is hindered by local haptic perturbations was carried out. The subjects could control the interaction compliance using the coactivation of a wrist antagonist muscles pair. We observed that subjects adapted their wrist activation pattern and cocontraction magnitude to cope with perturbations of variable intensity. The results confirmed an active regulation of the wrist viscoelasticity to reduce the tracking error. The CNS can selectively adjust muscle impedance to tune haptic interactions with the environment by learning a novel activation strategy.

Contribution Statement

The content of Chapter 3 has been developed by Gerolamo Carboni, with the contribution of Atsushi Takagi and Etienne Burdet.

The contributions are as follows:

- GC, AT, EB conceptualised the experiment.

- GC carried out the experiment.

- GC performed the data analysis.

3.1 Introduction

The central nervous system integrates the information flow of sensory stimuli to plan and perform consecutive motor responses which, in turn, alter the available information [55]. The mutual relationship entangling sensory inputs and motor commands with the surrounding environment is defined *perception-actuation loop* [23] and it is built through an *enactive approach* [56]. When guided by a dog, should one rigidly hold the leash to best know where it is going, or relax to filter its movement jerk? Previous studies on interacting with unpredictable dynamics [29], [39] suggest that one may stiffen the limbs to attenuate the disturbance. On the other hand, being rigidly connected could inject more noise into the system, or may provide more accurate information about its movement [15]. If one's motion is perturbed, such as when a dog abruptly pulls the leash so that the owner's arm reaches the limit of its range of motion, despite the intrinsic dynamics of a physical system can be exploited to facilitate the control of the system itself [24], an increase in cocontraction due to the joined action of reflexes and muscle mechanics [31] would disturb the owner's motion.

The results presented in Chapter 2 show that the CNS is able to adapt muscle cocontraction in order to attenuate the effect of a uniform displacement while dealing with the accuracy of visual and haptic information in an optimal fashion. As a following step, here we investigate to which extent the CNS can adapt the muscle activation to improve task performance when the required activation pattern is opposite to the one naturally framed by the muscle mechanics.

For this purpose, we developed a paradigm in which subjects tracked a visual target while being elastically connected to it. Subjects were required to track a complex but smooth function with wrist flexion/extension movement while the elastic force provided by the robotic interface was designed to hinder their performance through local impulsive haptic disturbances: tailored displacements of the elastic force reference were produced around the visual target's changes of direction (Fig. 3-1A), thus generating large acceleration and deceleration associated to a high level of cocontraction [57]. We thoughtfully investigated how the subjects deal with a trade-off between gaining target trajectory related information and attenuating the effect of perturbation. Also in this case, the experiment population could control the band elasticity by cocontracting the same pair of wrist muscles involved in tracking. Would subjects increase cocontraction to better use motion guidance, relax to attenuate the effect of haptic noise or combine the two behaviours as more convenient? As a consequent question, would they modify their muscle activation strategy, defined as muscle cocontraction timing and magnitude, to improve task performance?

Our *first hypothesis* is that the cocontraction would increase in magnitude when the haptic feedback is assisting the task completion and would attenuate for filtering out the noise otherwise. Given what we have observed in Fig. 2-4, where the local increase of cocontraction was the outcome of a change in tracking direction, the experiment was planned to deliver impulsive disturbances at the timing in which the users' muscle activation is the highest. Therefore, our *second hypothesis* is that the tracking strategy would adapt to reduce the noise impact, thus updating well established muscle activation patterns for boosting performance.

3.2 Methods

3.2.1 Subjects and experimental setup

The experiment was approved by the Research Ethics Committee of Imperial College London and carried out by 8 subjects (4 females) without known sensorimotor impairment

aged 25.62 ± 3.16 years old. Two subjects were left-handed. Each subject was informed about the experiment, gave informed consent, and filled in the Edinburgh handedness form [36] as well as a demographic questionnaire before starting with the experiment. Subjects carried out the experiment individually and each of them interacted with a single handle of the Hi5 dual robot [37], which is a 1-DOF flexion/extension wrist interface that can be controlled by both a human subject or robotic controller (Fig. 3-1A). The Hi5 interface was controlled at 1000 Hz, while wrist angle data was recorded at 100 Hz.

3.2.2 Muscle activation calibration and cocontraction computation

Surface electrodes were used to record EMG activity from the FCR and the ECRL muscles. This was calibrated through a process in which subjects were asked to flex/extend their wrist while their wrist was locked by the device at 0°, the subject's most comfortable position. The subject was asked to produce flexion and extension torques of 1, 2, 3 and 4 Nm for 2 s, first flexion then extension, with a rest period of 5 s between each activation to prevent fatigue. This EMG data was linearly regressed versus torque to estimate the relationship between muscular activity and torque. Then *cocontraction* was computed as

$$u(t) \equiv \min\{\tau_f(t), \tau_e(t)\}. \tag{3.1}$$

where $\tau_f(t)$ and $\tau_e(t)$ are the (absolute) flexor and extensor torque, computed from the respective EMG signals. The average cocontraction over all subjects was computed from each subject's normalised cocontraction, calculated as

$$u_n \equiv \frac{\overline{u} - \overline{u}_{min}}{\overline{u}_{max} - \overline{u}_{min}}, \quad \overline{u} \equiv \frac{1}{T}\int_0^T u(t)\,dt, \quad T = 20\,s \tag{3.2}$$

with $\overline{u}_{min}$ and $\overline{u}_{max}$ the minimum and maximum of the means of all trials of the specific subject.

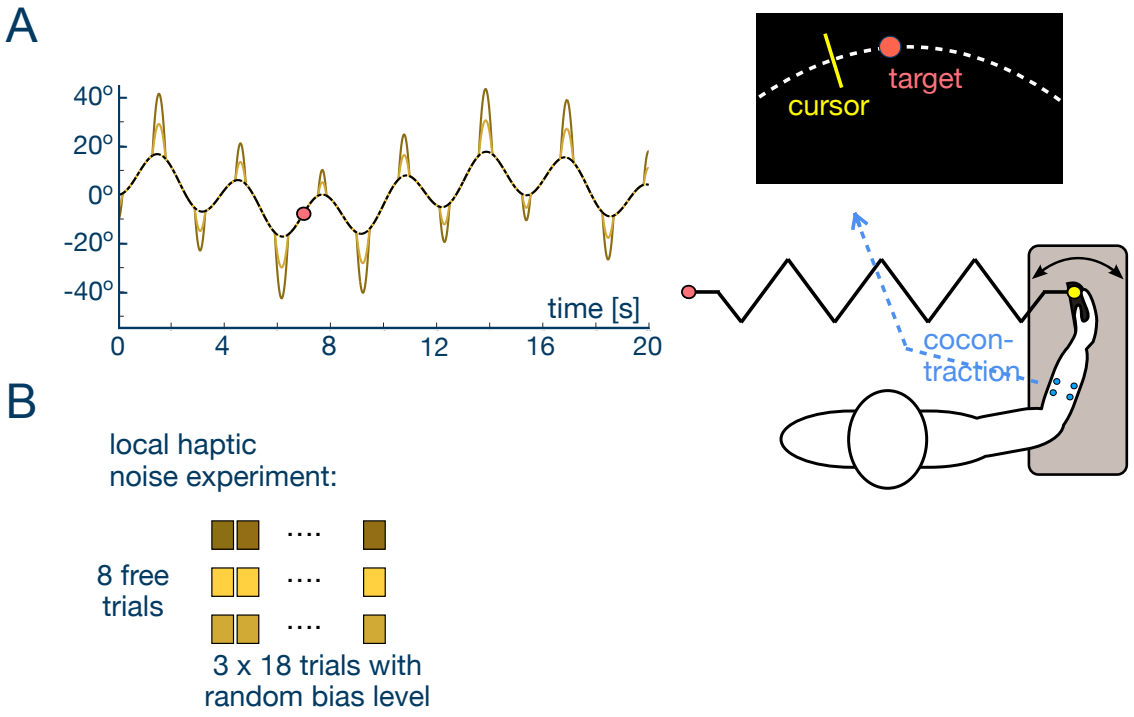

Figure 3-1: **Experimental framework for local perturbations.** (A) The subject uses wrist flexion/extension to track a sharp visual target while coupled with the haptic target characterised by an increasing haptic disturbance respectively for $\beta \in \{0, 2.5, 5\}$. The perturbations occur at about the moment in which the target changes direction. The black dashed line represents the user's visual target, corresponding to null mismatch. (B) Protocol for the experiment consisting in 3 randomised sets of 18 consecutive trials each.

3.2.3 Experimental protocol

Each subject was asked to track a visual pseudo-randomly moving target, being displayed on a screen in front of the user, "as accurately as possible" by using the wrist flexion/extension of their dominant hand. The target trajectory (in degrees) was given by

$$q^*(t) \equiv 12.7 \sin\left(\frac{\pi t^*}{2.547}\right) \sin\left(\frac{\pi t^*}{3.875}\right), \quad t^* \equiv t + t_0\,, \quad 0 \le t \le 20\,s \tag{3.3}$$

with t^* starting in each trial from a randomly selected zero $\{t_0 \in [0,20]\,\mathrm{s} \mid q^*(t_0) \equiv 0\}$, while being connected by the elastic force of equation (2.6) to

$$q_h(t) \equiv \begin{cases} q^*(t) & |\ddot{q}^*(t)| < \xi \equiv 35^\circ/s^2 \\ q^*(t) - \beta\,\mathrm{sign}[\ddot{q}^*(t)]\,(|\ddot{q}^*(t)| - \xi)\,. \end{cases} \tag{3.4}$$

This experiment investigates the adaptation to a local haptic perturbations profiled for hindering the tracking when the target changes direction and supporting it elsewhere (Fig. 3-1A). The visual reference trajectory has been slowed down when compared to the one proposed in Chapter 2 with the purpose of facilitating the subjects in finely controlling their muscle activation while tracking. This precaution has occurred after noticing that the subjects capability to modulate cocontraction within a trial was limited by the minimal activation due to keep it up with the tracking. The tracking performance, being displayed on the monitor at the trial's completion, was evaluated using the *tracking error* introduced with equation (2.5), where $q(t)$ denotes the joint angle of the interface at time t.

The experiment protocol is described in Fig. 3-1B and consists of a total 62 trials. In the initial *free phase*, each subject attempted 8 tracking trials without haptic feedback to familiarise with the task and minimise subsequent learning effects. It was followed by a 54 trials *interaction phase* split into 3 set of trials. Each set consisted of 18 consecutive trials with one of the three disturbances set by $\beta \in \{0, 2.5, 5\}$, where the three sets were carried out in random order by the different subjects.

3.3 Experimental results

For an exhaustive examination of the adaptation taking place withing the experiment, the measurements collected over time across the experimental blocks and the mean of the initial and final 6 block, are presented for each experimental condition. Given the limited number of subjects available for this experiment, non-parametric analyses were preferred over parametric ones when the data distribution was not normal. The statistical analyses presented in this section are therefore exact sign-test or paired-sample t-test for single pairs of observations and Freedman test or two-way repeated measures ANOVA when considering the effect of learning and the haptic condition as factors. The statistical significance was set at 5% with Tukey's HSD correction for all post-hoc comparisons.

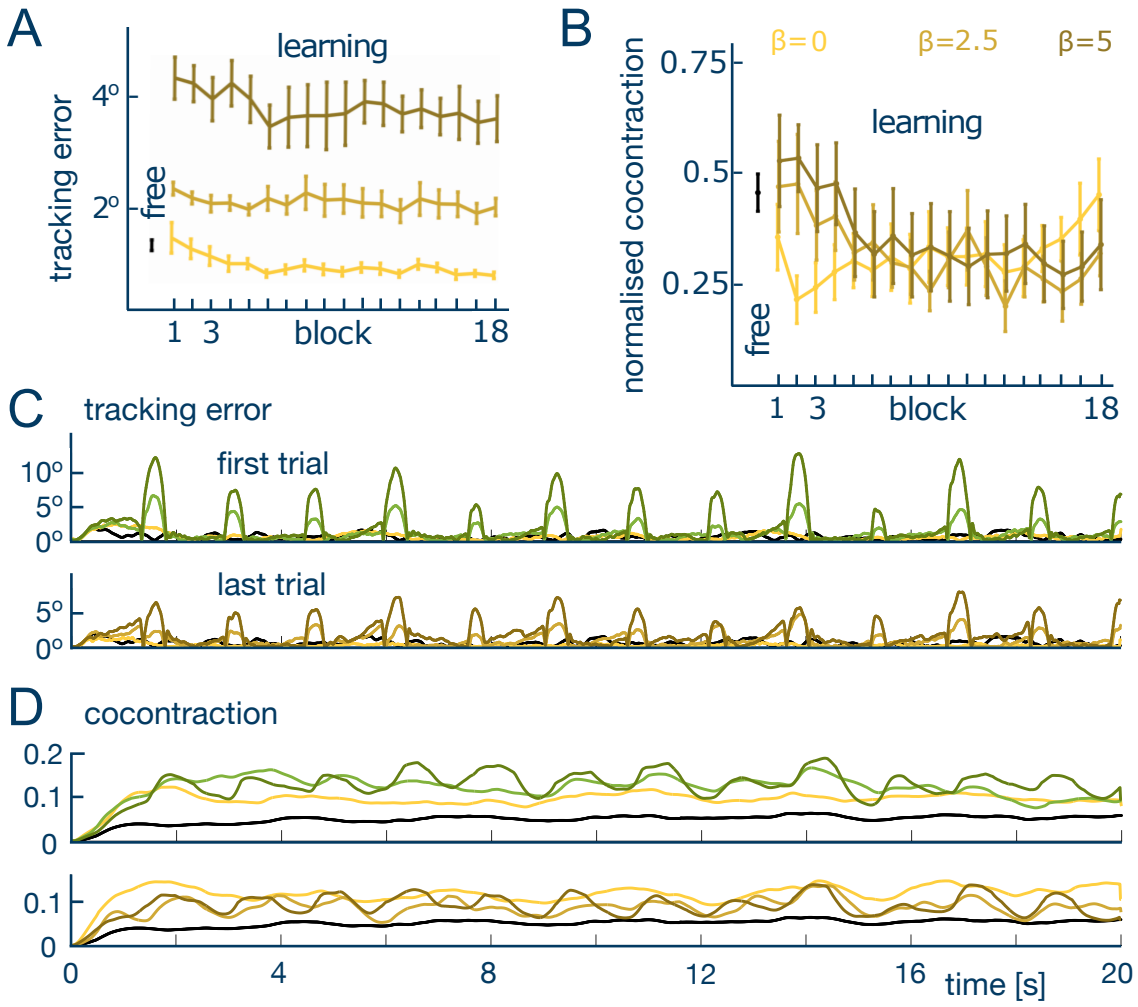

Figure 3-2: **Tracking error and muscle cocontraction adaptation.** (A) Mean tracking error values over blocks for the different haptic conditions. The performance improves with learning across perturbations of different magnitude. (B) Mean normalised muscle cocontraction over blocks for the different haptic conditions. The cocontraction increases for assistive haptic feedback and decreases when hindered by local perturbations. (C) Subject's average tracking error for the first (green lines) and the last (yellow to brown lines) experimental trials of each condition. The error drops around the turning points and increases in between. (D) The corresponding mean cocontraction adaptation. The muscle activation shrinks with learning in correspondence of local disturbances.

We initially analysed the tracking performance, presenting the subjects' mean tracking error and error deviation as function of the blocks number for the different haptic noise levels (see Fig. 3-2A). Since the very first trial of interaction, the perturbation magnitude was found to hinder the tracking performance in respect to the last free trial (Freedman non-parametric test, $\chi^2(3)=18.45$, $p<0.001$) with the exception of $\beta=0$, as confirmed by post-hoc comparison ($p=1$). The subjects improved their tracking while practicing the task

as indicated by a negative error slope (paired-sample t-test, t(7)=-3.15, p= 0.0160 for β=0; t(7)=-2.78, p=0.027 β=5). The performance analysis showed an after-training reduction of tracking error independent of the perturbation level (exact sign test between first and last block, p=0.0015). The tracking error in the last block was similarly affected by the haptic noise injected in the system (χ^2(3)=24, p<0.001). The post-hoc tests indicated a difference in the tracking performance for each combination of haptic conditions but when comparing the last free trial with β=0 and β=2.5 with β=5 (p=0.41).

In order to get an insight into the relationship between task performance improvement and muscle activation, we examined the mean cocontraction modulation over blocks (Fig. 3-2B). For an accurate and unbiased comparison among the population, cocontraction was normalised with respect to each subject's individual maximal recorded voluntary activation. The experimental data revealed that the cocontraction magnitude scaled up with respect to the last free trials after the introduction of haptic perturbations in the first block, as predicted by spontaneous disturbance minimisation through impedance control (χ^2(3)=15.45, p=0.0015; post-hoc analysis among interaction trials, p>0.76). Importantly, the last block of trials showed higher muscle cocontraction than the initial block in the case of null displacement at the turning points (β=0) and an homogeneous decrease in activation for $\beta \in \{2.5, 5\}$, therefore suggesting an updated interaction modulation. A significant proof of task adaptation can emerge from the comparison of cocontraction slopes across experimental blocks for the three proposed haptic scenarios (paired-sample t-test, t(7)=2.42, p=0.046 for β=(0,2.5); t(7)=9.53, p<0.001 for β=(0,5); t(7)=-0.27, p=0.79 for β=(2.5,5)). Coherently with our first hypothesis, the subjects were able to adapt their cocontraction to the local disturbances by increasing the cocontraction magnitude for assistive haptic feedback and decreasing it otherwise, thus confirming the trend discussed in the previous chapter.

As a following step in understanding the decrease of tracking error between the initial and final blocks for each experimental condition, the tracking profiles were inspected (Fig. 3-

2C). The improvement in performance appears to be a consequence of the error decreasing around the visual target turning points. The average error decreased by 0.42°, 0.59° and 1.71° for growing perturbation amplitude (paired-sample t-test, t(7)=4.06, p=0.005 for β=0; t(7)=2.19, p<0.064 for β=2.5; t(7)=3.12, p=0.017 for β=5). Interestingly, for post-training trials the mean tracking in between consecutive turning points became less accurate of respectively 0.11° and 0.33° for $\beta \in \{2.5, 5\}$ when compared with the initial block. Conversely, on average the task execution still improved of 0.34° for β=0 (t(7)=2.91, p=0.022). Could these results be explained as the outcome of an updated cocontraction strategy? The wrist muscle activation for the same trials was hence examined. As we see in Fig. 3-2D, with practice the muscle activation was finely controlled to attenuate perturbations. The normalised cocontraction pattern when connected to local disturbacnces was initially above the cocontraction level characterising an assistive coupling of 0.11 and 0.13 for $\beta \in \{2.5, 5\}$ (see light and dark green lines in Fig. 3-2D) and accordingly decreased lower to this level of about 0.12 and 0.10 (brown lines in Fig.3-2D, χ^2(2)=2242, p<0.001). Moreover, the patterns characterising activation in both solo and unperturbed trials (β=0) differ in shape when compared with the corresponding perturbed trials: since the first interacting block we could find signs of adaptation to the hindering coupling in the rise of the cocontraction frequency across the different experimental conditions ($f \in \{0.05, 0.15, 0.10, 0.65\} Hz$, Fast Fourier Transform for last free trial and increasing values of β respectively).

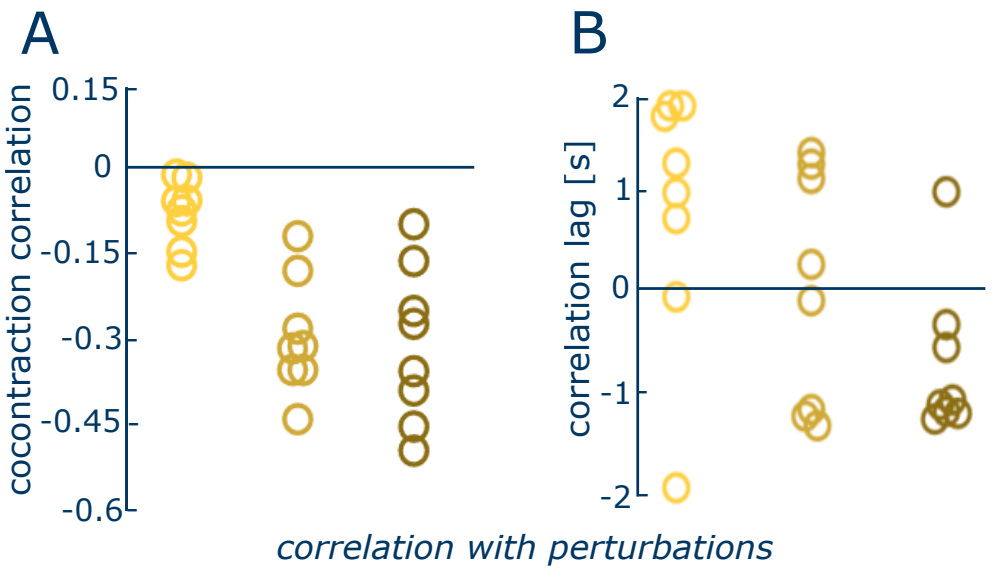

Figure 3-3: **Cocontraction correlation with perturbation patterns.** (A) Normalised cross-correlation between cocontraction minima and perturbation maxima in the final block. (B) Temporal lag between cocontraction and perturbation patterns for maximising the inverse correlation.

Fig. 3-3 shows that, in particular after learning, the minima of the cocontraction correlate with the perturbation maxima. Cross-correlations analyse the relationship between the perturbation dynamics and the subject's concurrent cocontraction. It was calculated as the time lag at which the correlation between the target and subject's positions was the lowest. A normalised cross-correlation exhibits mean correlation values of -0.07, -0.30 and -0.32 for $\beta \in \{0, 2.5, 5\}$. The cross-correlation delay was of about 2s for β=0, being thus compatible with the visual target oscillations. The value settled at about 1s when the disturbance was delivered in an attempt to cocontract in antiphase with the trajectory motion. Figs. 3-4 A, B provide a more detailed outlook of how the cocontraction strategy is updated by comparing the averaged first six and final six blocks of interaction for a representative subject. From this point on, the results description will only consider $\beta \in \{0, 5\}$ given the correlation between β=(2.5,5) (Pearson correlation coefficient: r(7)=0.88, p<0.001). In addition to the change in muscle activation intensity, Figs. 3-4C, D highlights a non-trivial tuning of the cocontraction minima and maxima with respect to the perturbations' onsets. While there is not significant difference in the timing of muscle cocontraction among early and late trials minima (t(10)=-0.36,

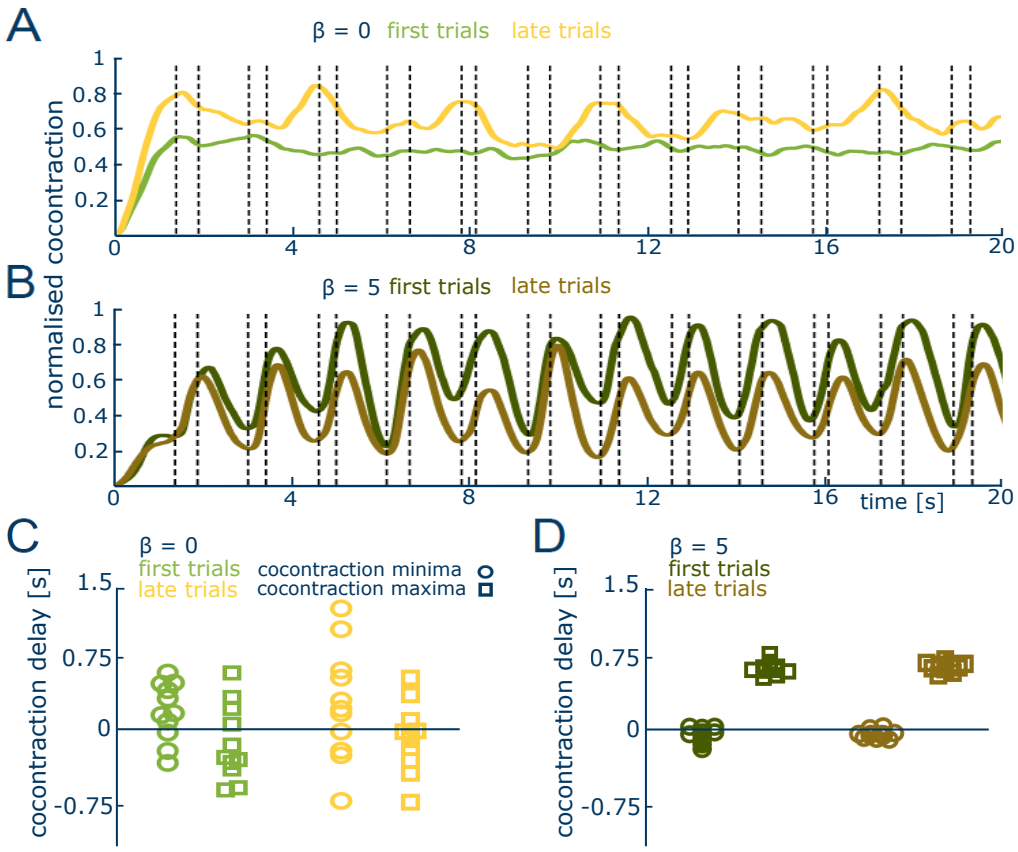

Figure 3-4: **Cocontraction adaptation: averaged results for a single representative subject.** (A) Normalised cocontraction pattern of a representative subject in the first six and last six blocks for β=0. Each couple of black dashed vertical lines represents the perturbations onset and ending. The activation pattern is tuned with learning and scales up in intensity. (B) Normalised cocontraction pattern of a representative subject in the first six and last six blocks for β=5. The cocontraction magnitude drops after task adaptation. (C) Delay of cocontraction minima (circles) and maxima (squares) with respect to the perturbations onset in the first six (in green) and last six (in yellow) blocks for β=0. The data points represent the subject behaviour with respect to each of the 11 perturbations characterising a trial. The cocontraction delay broadens for activation minima without substantially changing with learning. (D) Delay of cocontraction minima and maxima with respect to the perturbation onset in the first six (in green) and last six (in brown) blocks for β=5. The cocontraction keeps a consistent activation delay pattern while compacting the delay distribution around zero for the late blocks minima.

p=0.72), maxima t(10)=-0.10, p=0.92) and in between them (t(21)=1.96, p>0.078) when connected to an unperturbed trajectory, since early trials with local perturbations the subject learned to relax just before the perturbation onset and to cocontract again soon afterwards (t(10)=-24.85, p<0.001). This behaviour is strenghten by extra practice (t(10)=-50.24, p<0.001).

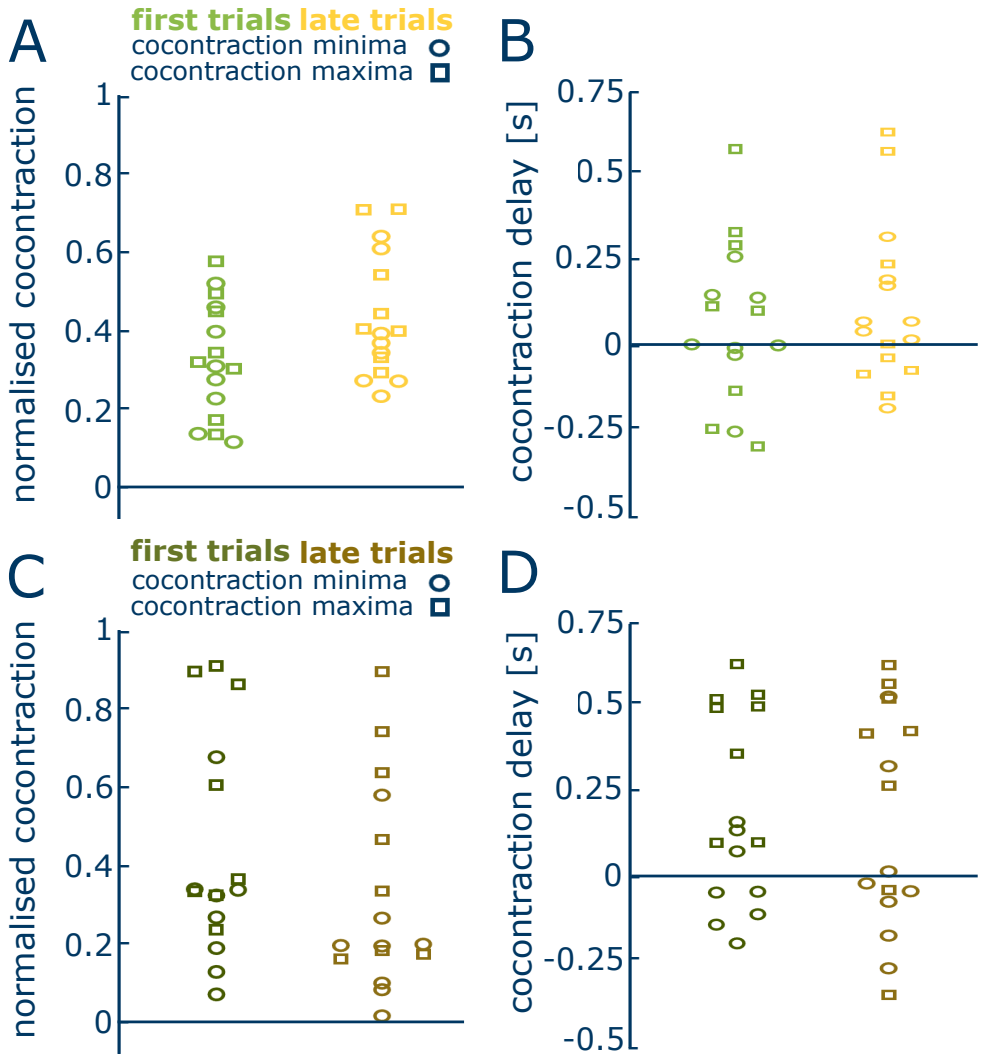

Figure 3-5: **Cocontraction adaptation: averaged population results.** (A) Normalised cocontraction minima (circles) and maxima (squares) with respect to the perturbation onset in the first six (in green) and last six (in yellow) blocks for β=0. The data points represent the individual subjects' mean behaviour averaged over the 11 perturbations characterising a trial. The normalised cocontraction is increased with training when coupled with an helpful haptic feedback. (B) Cocontraction delay with respect to the perturbations onset for β=0. The cocontraction delay does not mutate with training. (C) Normalised cocontraction minima (circles) and maxima (squares) with respect to the perturbation onset in the first six (in green) and last six (in brown) blocks for β=5. The cocontraction decreases with learning, as an attempt to mitigate the perturnation effect. (D) Delay of cocontraction with respect to the perturbation onset for β=5. The cocontraction delay is skewed with most of subjects trying to relax before the perturbation starts and then cocontracting afterwards. This effect becomes more consistet with learning.

The subjects general behaviour was found to be consistent with the proposed individual trend. Fig. 3-5A shows that the normalised cocontraction when coupled to the assistive guidance is increased for both minima and maxima ($F(1,7)=66.61$, $p<0.001$) with training ($F(1,7)= 7.92$, $p=0.025$) as confirmed with a two-way RANOVA. A significant interaction effect was found between cocontraction modulation and learning ($F(1,7)=17.69$, $p=0.004$). Conversely, no significant difference was found in the cocontraction timing between minima and maxima for both early and late trials (Fig. 3-5B). When considering β=5, the normalised cocontraction displays higher maxima and lower minima than the previously examined ones (Fig. 3-5C). Another two-way RANOVA confirmed the cocontraction being decreased with learning ($F(1,7)=50.45$, $p<0.001$), thus showing a significant reduction in activation before and after the perturbation onset ($F(1,7)=15.52$, $p=0.005$). Importantly, the cocontraction delay settled in two clusters ($F(1,7)=4.89$, $p=0.062$) with the subjects relaxing closer to the disturbance onset and increasing again muscle activation after its decay (Fig. 3-5D). Post-hoc comparisons supported the idea of a synchronisation to the perturbation with a significant difference in relaxations delay ($p=0.012$).

3.4 Discussion

The muscle activation evolution over time presented in the *guidance bias experiment* of Chapter 1 suggested that higher cocontractions were associated with tracking around the visual target changes of direction. The subjects stiffened their wrist conspicuously when the wrist run was approaching the end of its flexion/extension range of motion [31]. While for this task the wrist anatomy naturally helped in stabilising tracking when most needed, what would happen when the muscle mechanics is negatively affecting the task accomplishment?

In this chapter we explored whether humans could consciously reshape the muscle activation pattern established by their body morphology when helpful to improve their performance in a given task. To this purpose, we implemented a cocontraction dependent perturbation during the target's direction reversals. The results showed that subjects could reduce

their tracking error with training as consequence of a modified cocontraction muscle activation. Subjects relied more on the haptic reference when supportive and reduced their coupling when interfering with the task. They further learned to relax when approaching a perturbation and to cocontract again soon afterwards. This voluntary coupling modulation steamed from and updated activation strategy developed to maximise useful interactions and to minimise disturbances, as highlighted by the negative after-learning cross-correlation between cocontraction minima and perturbation maxima.

Altogether, these results further indicate that subjects can actively tune the coupling dynamics with the environment to maximise haptic information during physical interaction. In particular, the CNS modulates the body's mechanical impedance to enhance haptic sensing, thus filtering the useful kinesthetic information coming from the interaction in order to stochastically weight haptic information subjected to noise [15], [16], [20], [58]. Hence, the ability to fine-tune the interactional information may be a common factor in all interactive tasks and could determine how subjects use this information to their advantage. Critically, this study showed evidences of robust adaptation in humans with the CNS capability to take advantage of *adaptive sensing* not fading when constrained by body morphology and well established task dependant muscle activation patterns.

Chapter 4 Physically interacting humans regulate muscle cocontraction to improve visuo-haptic perception

---

Summary

When moving a piano or dancing tango with a partner, how should I control my arms to best feel my partner's movements and follow or guide them smoothly? In our study, we observed that physically connected pairs of subjects tracking a common target adapted the compliance of their wrists depending on both own and the partner's performance. The wrist's rigidity, as measured by muscular cocontraction, was more compliant when vision was blurred, and stiffened when the partner's performance was worse. Computational modelling revealed that this cocontraction adaptation cannot be explained by the movement error minimization proposed in earlier models. Instead, individuals skilfully regulate the arm's compliance to guide it along the planned motion while minimizing effort and gathering relevant haptic information from the interacting partner. The CNS regulates muscle cocontraction to guide motion by extracting maximal task information from vision and haptics while concurrently minimizing energy.

Contribution Statement

The content of Chapter 4 has been developed by Gerolamo Carboni*, with the contribution of Hendrik Börner*, Xiaoxiao Cheng*, Atsushi Takagi, Sandra Hirche, Satoshi Endo and

Etienne Burdet.

The contributions are as follows:

- GC, HB, SH, EB conceptualised the experiment.
- GC, HB carried out the experiment.
- GC, HB, AT, SE, EB performed data and statistical analysis.
- GC, HB, XC, EB developed the computational modeling.
- GC, HB, XC, AT, SH, SE, EB have edited the text and agree with its content.

This chapter's content has been submitted to *Science Advances* as: H. Börner*, G. Carboni*, X. Cheng*, A. Takagi, S. Hirche, S. Endo and E. Burdet. "Physically interacting humans regulate muscle cocontraction to improve visuo-haptic perception".

* equal contribution

4.1 Introduction: Why and what we do?

Human muscles are elastic elements that increase stiffness and shorten with activation [57]. While it was shown that the CNS regulates the limbs' stiffness by coordinating muscles' activation to shape the interaction with the environment [27], [29], [41], [42], how this affects haptic sensing is not known. When two connected individuals carry out a task together, such as when moving a piece of furniture or sharing the control of an old-school aircraft through a rigid cross-cockpit linkage [59] (Fig. 4-1A), they exchange haptic information about their motion plan to combine with own visual information and improve their accuracy [48]. During these physical interactions, it is unclear whether one should keep the arm relaxed or compliant so that can correct the motion more readily, or if one should cocontract its muscles and stiffen the arm for guiding the partner along its planned movement. As the quality of this haptic communication varies with the

connection stiffness [15], could humans regulate muscle cocontraction to adapt their limb stiffness and better sense the partner's movement?

To investigate how physically connected individuals adapt their limbs cocontraction, we observed 22 connected pairs of subjects or dyads tracking a common randomly moving target using wrist flexion and extension (Fig. 4-1A). The target observed by each partner on an individual monitor was either *sharp and precise* (a 8 mm large disk) or *noisy* (a dynamic cloud of 8 normally distributed dots). We analyzed the tracking performance and wrist cocontraction of each partner in four conditions: sharp (self) - noisy (partner) (SN), sharp - sharp (SS), noisy - sharp (NS) and noisy - noisy (NN) as described in the Methods section 4.2. The experiment was carried out as a within-subject design with these four *interaction conditions* randomly presented in a block of ten trials per condition (Fig. 4-1B). The forty interaction trials were preceded by five solo trials without interaction with the partner to learn the task, and followed with five solo trials.

Studies on the adaptation to unpredictable force fields [29], [39] suggest that muscle cocontraction would increase with the tracking error magnitude [41] independent of its source. However, in line with the results presented in the previous chapters, we *first hypothesize* that in our experiment the subjects would be able to adapt their muscle cocontraction to the level of visual noise in their own target and to haptic noise resulting from the interaction with the partner (with their own visual noise). Furthermore, it was observed in [60] that subjects cocontract with increased accuracy constraints. Therefore, our *second hypothesis* is that in presence of visual noise making it harder to ensure accurate tracking the subjects would increase cocontraction. Finally, we expected that the subjects would filter out the noise from a partner receiving fuzzy visual feedback of the task by reducing cocontration. Therefore, our *third hypothesis* is that cocontraction would decrease if the partner's target had more noise.

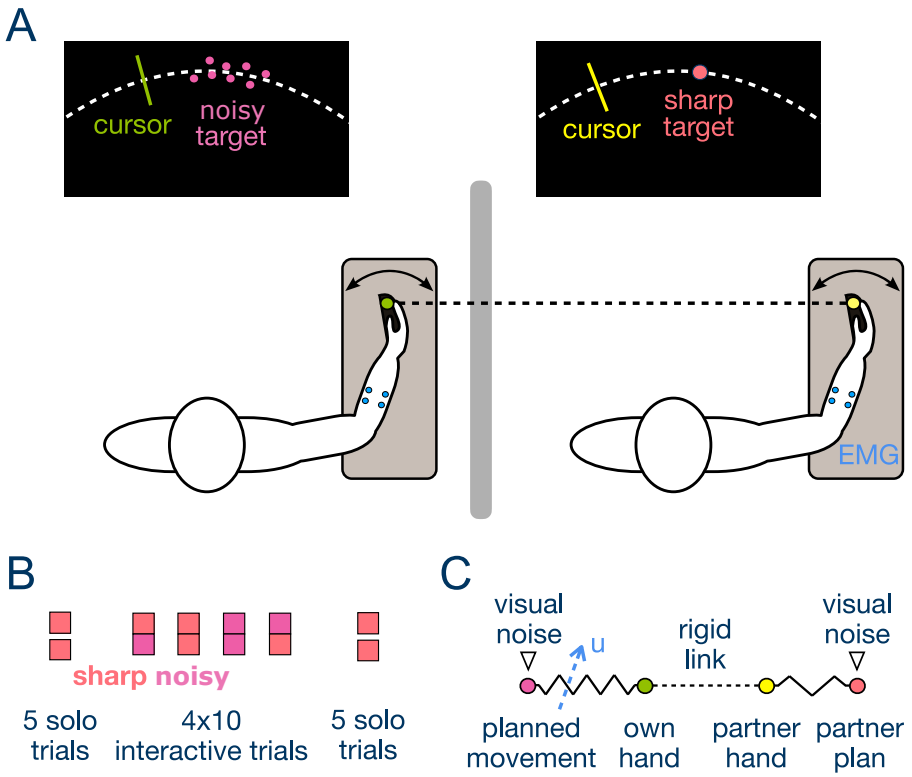

Figure 4-1: **Schematic of the experimental task and modeling.** (A) The two partners tracked the same randomly moving target with their wrist flexion-extension movement while being connected with a rigid virtual bar. Their wrist flexion/extension movement was recorded, as well as the myoelectrical activity of a flexor-extensor muscle pair. (B) Protocol of the experiment to study the effect of visual noise on either partner on performance and cocontraction. (C) Mechanical modeling of the interaction with the partner and with own movement plan. Both own and the partner movement plans are affected by the respective visual noise. The interaction with the partner's hand depends on the stiffness of the connection to their motion plan modulated by their cocontraction u.

4.2 Methods

4.2.1 Subjects and experimental setup

The experiment was approved by the Joint Research Compliance Office at Imperial College London. A total of 44 subjects without known sensorimotor impairments, aged 18–37 years, including 16 females, were recruited. Each subject gave written informed consent prior to participation. The majority of subjects were right-handed (37/44), as was assessed using the Edinburgh Handedness Inventory [36]. The subjects carried out the experiment in pairs or *dyads*, with 14 male-male dyads and 8 female-female dyads. The two subjects

of a dyad were seated comfortably on height-adjustable chairs, next to the Hi5 dual robotic interface. The system consists of two 1 DoF flexion/extension wrist interfaces where the subjects can lean their arms and easily hold a handle. This unique bilateral manipulandum-to-manipulandum system allows the two subjects to exchange interaction torques through the handle that each of them holds with their dominant wrist, as shown in Fig. 4-1A (further details on the Hi5 dual robotic interface can be found in [37]). A personal monitor placed in front of each subject provided them visual feedback of the task with a cursor indicating their own wrist position (Fig. 4-1A). No visual feedback of the partner's position was available as the two subjects were separated by a curtain, and they were instructed not to speak to each other during the experiment.

Each Hi5 handle is connected to a current-controlled DC motor (MSS8, Mavilor) that can exert torques of up to 15 Nm, and is equipped with a differential encoder (RI 58-O, Hengstler) to measure the wrist angle and a (TRT-100, Transducer Technologies) sensor to measure the exerted torque in the range [0,11.29] Nm. The two handles are controlled at 1 kHz using Labview Real-Time v14.0 (National Instruments) and a data acquisition board (DAQ-PCI-6221, National Instruments), while the data was recorded at 100 Hz.

The activation of two antagonist wrist muscles, FCR and ECRL were recorded during the movement from each subject. EMG signals were measured with surface electrodes using the medically certified g.Tec's g.LADYBird&g.GAMMABox&g.BSamp system. The EMG data was recorded at 100 Hz.

4.2.2 Tracking task

The two partners were required to track the same *visual target* (in degrees) moving with

$$q^*(t) \equiv 18.5 \sin\left(\frac{\pi t^*}{1.547}\right) \sin\left(\frac{\pi t^*}{2.875}\right), \quad t^* \equiv t + t_0\,, \quad 0 \leq t \leq 20\,s \tag{4.1}$$

as accurately as possible using flexion-extension movements (Fig. 4-1A). To prevent the subjects from memorising the target's motion, t^* started in each trial from a randomly

selected zero $\{t_0 \in [0,20]\,\mathrm{s} \mid q^*(t_0) \equiv 0\}$ of the multi-sine function. The respective *tracking error*

$$e \equiv \left(\frac{1}{T}\int_0^T [q^*(t) - q(t)]^2\, dt\right)^{\frac{1}{2}},\ \ T \equiv 20\,s \tag{4.2}$$

was displayed at the end of each 20 s long trial.

After each trial, the target disappeared and the subjects had to place their respective cursor on the starting position at the center of the screen. The next trial then started after a 5 s rest period and a 3 s countdown. The initialization of next trial started when both subjects placed their wrist on the starting position, so that each subject could take a break at will in between trials, by keeping the cursor away from the center of the screen.

4.2.3 Experimental conditions and protocol

In *solo trials*, the two partners moved the wrist independently to each other. In *interactive trials*, the partners' wrists were connected by a stiff virtual spring with torque (in Nm)

$$\tau(t) = 17.2\,[q_p(t) - q_o(t)]\,, \tag{4.3}$$

where q_o and q_p (in radians) denote own and the partner's wrist angles. As the tracking errors of the two partners of a dyad were strongly correlated ($r(20)=0.95$, $p<0.0005$), the average tracking error between them was used in the data analysis.

The interaction trials were carried out under two different visual feedback conditions. In the *sharp condition* the target visual was displayed as a single 8 mm diameter disk. In the *noisy condition* the target trajectory was displayed as a "cloud" of eight normally distributed dots around the target. The cloud of dots were defined by three parameters, randomly picked from independent Gaussian distributions: the vertical distance to the target position $\eta \in \mathrm{N}(0, 15\,\mathrm{mm})$, the angular distance to the target position $\eta_q \in \mathrm{N}(0, 4.58^\circ)$, and the angular velocity $\eta_{\dot{q}} \in \mathrm{N}(0, 4.01^\circ/\mathrm{s})$. Each of the eight dots was sequentially replaced every 100 ms.

A calibration of the measured EMG (described in Section 4.2.4) was first carried out to map the raw EMG signal (in mV) to a corresponding torque value (in Nm), so that the activity of each subject's flexor and extensor's can be compared and combined in the data analysis. After this calibration, the subjects carried out 5 initial solo trials to learn the tracking task and the dynamics of the wrist interface. This was followed by 4 blocks of 10 interaction trials, each with one of the different noise conditions {noisy (self)-sharp (partner), SN, SS, NN} presented in a random order, followed by 5 control solo trials (Fig. 4-1B). The subjects were informed when an experimental condition would be changed but not which condition would be encountered in the next trials.

4.2.4 Muscle activation calibration and cocontraction computation

The subjects placed their wrist in the most comfortable middle posture, set to 0°. Constrained at that posture, they were then instructed to sequentially (*i*) flex or extend the wrist to exert a torque, or (*ii*) maximally co-contract in order to keep the wrist position stable during a 3 Hz sinusoidal positional disturbance of 10° amplitude. Each phase was 4 s long and was followed by a 5 s rest period to avoid fatigue. The latter period was used as a reference activity in the relaxed condition. This procedure was repeated four times at flexion/extension torque levels of {1,2,3,4} Nm and {-1,-2,-3,-4} Nm, respectively. For each subject, the recorded muscle activity was then linearly regressed against the torque values to estimate the relationship between them. The raw EMG signal was first high-pass filtered at 20 Hz using a second-order Butterworth filter to remove drifts in the EMG signal. This was then rectified and passed through a low-pass second-order Butterworth filter with a 5 Hz cut-off frequency to obtain the envelope of the EMG activity.

The torque of the flexor muscle could then be modelled from the envelope of the EMG activity u_f as

$$\tau_f(t) = \alpha_0 u_f(t) + \alpha_1, \quad \alpha_0, \alpha_1 > 0, \tag{4.4}$$

and similarly for the torque of the extensor muscle τ_e. *Muscle cocontraction* was then computed as

$$u(t) \equiv \min\{\tau_f(t), \tau_e(t)\}. \tag{4.5}$$

The average cocontraction over all subjects (as shown in Fig. 4-3) was computed from each subject's normalised cocontraction, calculated as

$$u_n \equiv \frac{\overline{u} - \overline{u}_{min}}{\overline{u}_{max} - \overline{u}_{min}}, \quad \overline{u} \equiv \frac{1}{T}\int_0^T u(t)\,dt, \quad T \equiv 20s \tag{4.6}$$

with $\overline{u}_{min}$ and $\overline{u}_{max}$ the minimum and maximum of the means of all trials of the specific subject.

4.2.5 Simulation of tracking error minimization (TEM)

For each of the 4 noise conditions $(i,j) \in \{\text{SS}, \text{SN}, \text{NS}, \text{NN}\}$, the initial cocontraction level $\{\hat{u}_{i,j}(1)\}$ was set as the initial experimental value $\{u_{i,j}(1)\}$. Then, by using the respective trial-by-trial tracking error $\{e_{i,j}(k)\}, k = 1, ..., 10$ from the experiment, the adaptation parameters α, γ in the computational model of eq.(4.14) were computed to minimize the error between the learned cocontraction values after 9 iterations $\{\hat{u}_{i,j}(10)\}$ and the corresponding data $\{u_{i,j}(10)\}$ in last experiment's trial:

$$(\alpha^*, \gamma^*) \equiv \arg\min_{\alpha,\gamma}\left\{\sum_{i,j}\left[\hat{u}_{i,j}(10) - u_{i,j}(10)\right]^2\right\}. \tag{4.7}$$

The parameters $\alpha^* \equiv 0.5, \gamma^* \equiv 0.06$ were found by using a grid search with a step 0.01 in the range $[0,2] \times [0,1.5]$.

4.2.6 Simulation of planning noise minimization (PNM)

Using the standard deviation of own visual noise $\sigma_o \in \{0, 4.58^\circ\}$ in each noise conditions, the adaptation parameters α, ζ, γ in the computational model of eq. (4.15) were identified that minimize the error between the learned values $\{\hat{u}_{i,j}(10)\}$ and the last trial's data

$\{u_{i,j}(10)\}$:

$$(\alpha^*, \zeta^*, \gamma^*) \equiv \underset{\alpha,\beta,\gamma}{\arg\min} \left\{ \sum_{i,j} \left[\hat{u}_{i,j}(10) - u_{i,j}(10) \right]^2 \right\}. \tag{4.8}$$

The parameters $\alpha^* \equiv 0.01$, $\zeta^* \equiv 0.1$, $\gamma^* \equiv 0.2$, were determined by using a grid search with a step 0.01 in the range $[0,2] \times [0,2] \times [0,1.5]$.

4.2.7 Simulation of optimal information and effort (OIE)

A gradient descent optimisation was used to minimize the prediction error and effort $V(u) = E(u) + \frac{1}{2}\gamma u^2$ with $E(u)$ defined in eq. (4.16). Muscle cocontraction was updated trial after trial using:

$$\begin{aligned} u_{new} &= u - \frac{dV(u)}{du} = -\frac{dE(u)}{du} + (1-\gamma)\,u\,, \\ -\frac{dE(u)}{du} &= \left[\frac{\sigma_p^2}{\sigma_o^2 + \sigma_p^2} \right]^2 \left[-\frac{d\sigma_o^2(u)}{du} \right] > 0\,. \end{aligned} \tag{4.9}$$

The target tracking arises from the guidance to the planned motion and the mechanical connection with the partner, with both being subjected to the noise in the individual's visual feedback (Fig. 4-1C). How should σ_o be modelled? Let σ_{vo} describe the tracking deviation of own wrist movement due to the target cloud. The wrist's compliance also affects the tracking performance and adds to this noise in the planned movement [15]. Assuming that these two effects are independent and that the wrist's viscoelasticity results in zero mean noise with deviation $\sigma_{\kappa o}(u)$, the deviation in the wrist can be calculated as

$$\sigma_o^2(u) = \sigma_{vo}^2 + \sigma_{\kappa o}^2(u)\,. \tag{4.10}$$

The effect of the connection noise was identified in [61] from a tracking experiment in which subjects were guided only from haptic feedback (thus without visual feedback), as

$$\sigma_{\kappa o}(u) = \xi_0 + \xi_1\, e^{-\beta_\kappa u} \quad \xi_0, \xi_1, \beta_\kappa > 0 \tag{4.11}$$

with $\xi_0 = 5.18$, $\xi_1 = 49.65$, $\beta_\kappa = 6.11$.

In the experiment, own visual noise and the partner's noise on the wrist movement each have two values, resulting in four parameters to identify for each model: $\{\sigma_{vo}^{(0)}, \sigma_{vo}^{(n)}, \sigma_p^{(0)}, \sigma_p^{(n)}\}$, where (0) represents the clean target while (n) corresponds to the cloud target. These parameters, used in the noise models of eqs.(4.10, 4.11), were computed by minimizing the variation of the cost derivative:

$$\left(\sigma_{vo}^{(0)*}, \sigma_{vo}^{(n)*}, \sigma_p^{(0)*}, \sigma_p^{(n)*}\right) \equiv \tag{4.12}$$
$$\underset{\sigma_{vo}^{(0)}, \sigma_{vo}^{(n)}, \sigma_p^{(0)}, \sigma_p^{(n)}}{\arg\min} \left\{ \sum_{i,j} \left[\frac{\partial V}{\partial u} \left(\hat{u}_{i,j}(10),\, \sigma_{vo}^{(i)},\, \sigma_p^{(j)} \right) \right]^2 \right\}$$

Using the learned cocontraction data $\{\hat{u}_{i,j}(10)\}$, a grid search for $(\sigma_{vo}^{(0)}, \sigma_{vo}^{(n)}, \sigma_p^{(0)}, \sigma_p^{(n)})$ in $[0,10] \times [0,20] \times [0,10] \times [0,20]$ with step 0.2 yields $\sigma_{vo}^{(0)*} = 10$, $\sigma_{vo}^{(n)*} = 18.8$, $\sigma_p^{(0)*} = 5.2$, $\sigma_p^{(n)*} = 6$, where for each gridpoint $\gamma^* = 0.65$ was the solution of

$$0 \equiv \frac{d}{d\gamma} \left(\sum_{i,j} \left[\frac{\partial V}{\partial u} (\hat{u}_{i,j}(10), \sigma_{vo}^{(i)}, \sigma_p^{(j)}) \right]^2 \right). \tag{4.13}$$

4.3 Experimental results

To evaluate the short-term adaptation within each condition, the measurements from the first half and the second half of trials were averaged into two epochs for the statistical analysis.

As the two partners of a dyad are rigidly connected, the root mean square *tracking error* by trial was analysed per dyad using a two-way repeated-measures ANOVA with noise conditions {SS, NN, SN $\equiv$ NS since $r(20)$=0.95, p<0.0005} and epoch as the factors. Statistical significance was detected at 5% with Bonferroni correction for all post-hoc comparisons. As *muscle cocontraction* was modulated by each partner, it was analysed individually wherein the partner's visual noise was perceived as haptic noise. Thus, a

three-way repeated-measures ANOVA with visual noise, haptic noise and epoch as the factors was used in the cocontraction analysis.

Fig. 4-2 shows that the tracking error decreased in the initial solo trials, and the learning had saturated by the last of the initial solo trials to the same degree as the average of the last solo trials (paired-sample t-test, t(21)=0.354, p=0.73). The analysis of error in the different noise conditions indicated that the magnitude of the tracking error depended on the noise level (F(1,21) = 91.95, p<0.001, η_p^2=0.81). The post-hoc comparisons showed that the tracking error in the mixed noise condition $\{\mathrm{SN} \equiv \mathrm{NS}\}$ was greater than in the SS condition (p<0.001) and smaller than in the NN condition (p<0.001). The tracking error remained at a similar level between the first and the second epochs (p=0.64), and there was no interaction effect between the noise level and epoch (p=0.17).

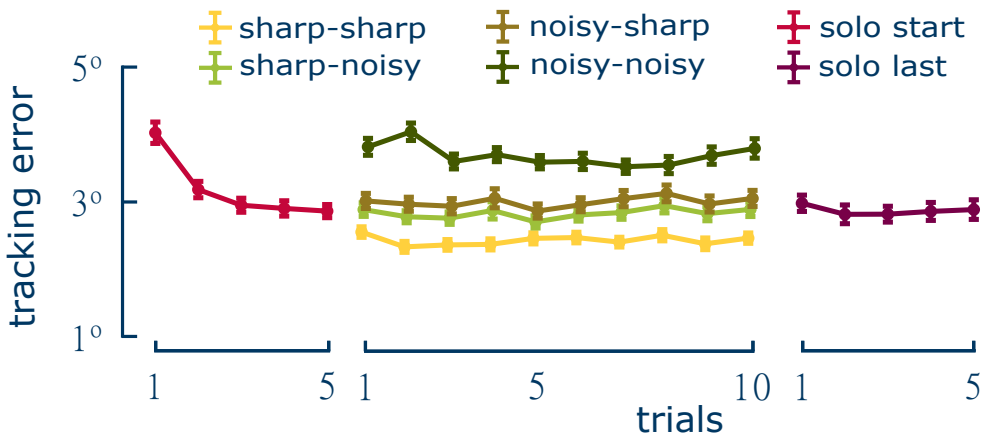

Figure 4-2: **Evolution of tracking performance in different noise conditions.** Error bars with standard error. Group mean tracking error charted as a function of trials. The error saturated in the initial solo trials, and increased with visual and haptic noise.

The cocontraction level decreased with the epoch (F(1,43)=53.58, p<0.0005, η_p^2=0.56), similar to what was observed during the learning of a novel force field [40], [41] (Figs. 4-3, 4-4). There was an interaction effect between visual noise and epoch (F(1,43)=15.65, p<0.001, η_p^2=0.27), and no significant interaction was found between haptic noise and epoch (p=0.21). The reduction in the cocontraction thus occurred at a slower rate than the

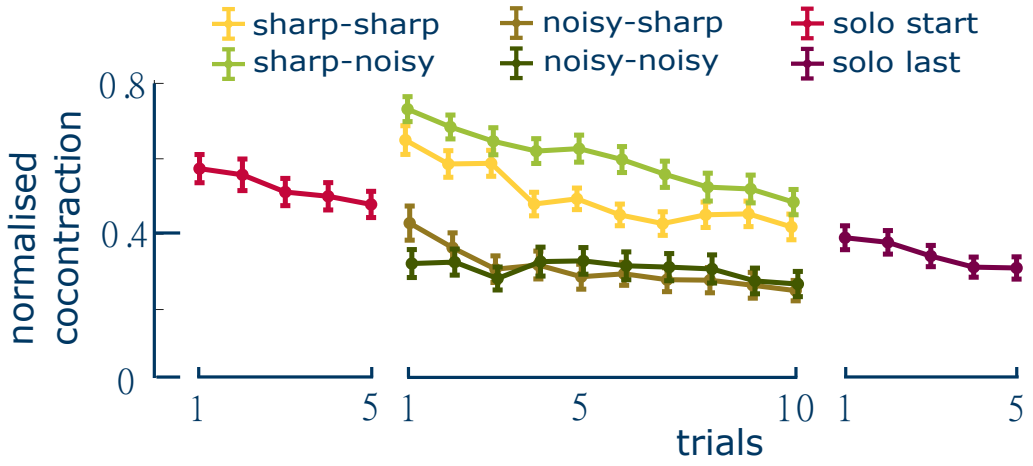

Figure 4-3: **Evolution of cocontraction in different noise conditions.** Error bars with standard error. The normalized cocontraction as a function of trials. The cocontraction decreased across all noise conditions, while visual noise tended to affect the cocontraction by a larger margin than the haptic noise.

change in the movement error, an observation consistent with the outcomes of force field learning [30].

Importantly, the cocontraction decreased with a larger level of own visual noise ($F(1,43)=85.91$, $p<0.0005$, $\eta_p^2=0.67$) while it increased with haptic noise from the interaction with the partner ($F(1,43)=5.53$, $p<0.03$, $\eta_p^2=0.11$). Post-hoc comparisons confirmed that all differences between the combinations of the visual and haptic noises were significant with the exception of NS vs. NN ($p=0.99$). Visual noise had a larger effect on cocontraction than haptic noise. Augmenting visual noise decreased the cocontraction by 0.194 when the haptic noise was low (i.e. NS-SS) and 0.293 when the haptic noise was high (NN-SN), while the cocontraction increased by only 0.100 when haptic noise increased with high visual noise (NS-NN) and 0.001 with low visual noise (SS-SN).

These results demonstrate that during interaction, the CNS spontaneously regulates muscle cocontraction considering the level of the visual noise on one's own and the partner's targets, in agreement with our first hypothesis. However, the observed cocontraction patterns contradict the second and third hypotheses as cocontraction decreased largely

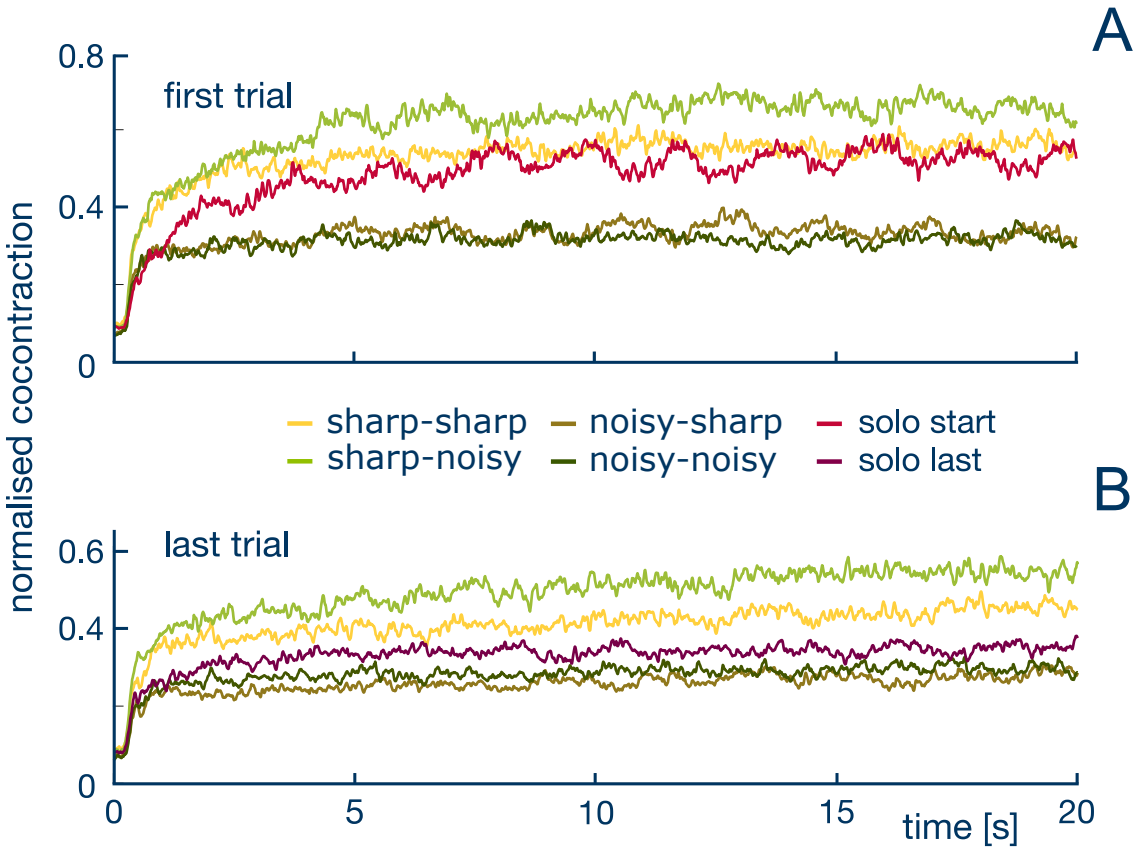

Figure 4-4: **Cocontraction adaptation during interaction trials.** Cocontraction waveforms during interaction trials with different noise conditions in the first (A) and last (B) trials' blocks. While the normalised cocontraction decreased with practice for each experimental condition, the cocontraction drop was limited when the subjects tracked a noisy target.

with own visual noise and increased slightly with the haptic noise stemming from the visual noise at the partner.

4.4 Computational adaptation mechanism

To clarify the cocontraction adaptation mechanism during interaction, we first tested the computational model of [41] that explains the motor learning in novel force fields. In this model, the cocontraction u increases with each new trial to minimize tracking error e, and decreases to minimize effort, according to

$$u_{new} \equiv \alpha e + (1-\gamma) u, \quad \alpha, \gamma > 0. \tag{4.14}$$

Simulation of the learning during the ten trials of each condition with this *tracking error minimization* (TEM) model predicted cocontraction at a level increasing with the corresponding tracking error (Fig. 4-5A). This prediction is qualitatively different from the data, such as larger cocontraction in the noisy relative to the sharp visual feedback condition (e.g. compare the NN and SS conditions in Fig. 4-5A). Therefore, the TEM model cannot explain the adaptation in the cocontraction during interaction.

We considered what adaptation factor may be missing from the TEM model. The statistical analysis revealed that own visual noise was a major factor of the cocontraction level adaptation. A larger cocontraction level increases the stiffness of the wrist, thereby strengthening the guidance to the planned movement (Fig. 4-1C). However, if the planned movement is disturbed by visual noise, a stiffer connection will bring larger noise to the hand control, in which case it would be better to relax the arm. Therefore, cocontraction u should decrease with visual noise deviation $\sigma_o(u)$:

$$u_{new} \equiv -\alpha\,\sigma_o + \zeta + (1-\gamma)\,u\,, \quad \alpha,\zeta,\gamma > 0\,, \tag{4.15}$$

counterbalanced by a general increase ζ and effort minimisation. Simulation with this *planning noise minimization (PNM)* model yields a trend similar to the data, with cocontraction decreasing in the NS and NN conditions (Fig. 4-5A). However, the PNM model is not able to differentiate between these two conditions or between the SS and SN conditions.

This result suggests that cocontraction adaptation depends not only on own visual noise but also on the haptic noise from the partner. As illustrated in Fig. 4-1C, the hand's movement depends on the guidance towards the planned movement and on the connection to the partner. As the stiffness of the guidance increases with own cocontraction [27], it is in principle possible to weight these two influences. Cocontraction should decrease to lower the guidance to the planned movement when it is affected by visual noise. Conversely, the guidance to the planned motion should increase to counteract the effect of haptic noise when the partner receives noisy visual feedback. The experimental data

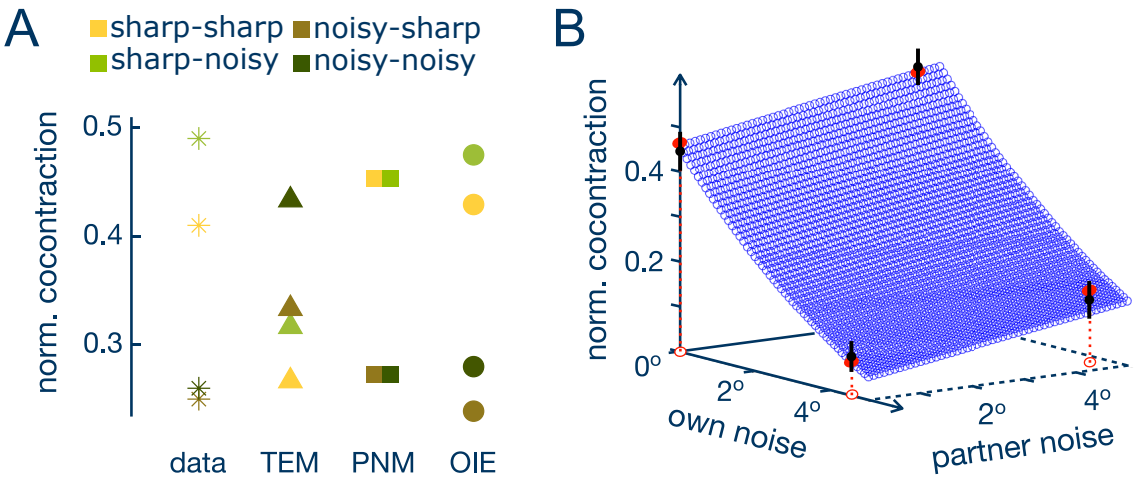

Figure 4-5: **Results of computational modeling the cocontraction adaptation to own and partner noise.** (A) Comparison of cocontraction predicted by the three models described in the text. The TEM model predicts a different modulation of cocontraction with varying noise conditions as in the data, the PNM model predicts only the modulation with own visual noise. (B) The OIE model prediction (red ovals) exhibits a similar decrease of cocontraction with own noise and increase with partner noise as in the data (black disks with standard error bars).

of Fig. 4-3 seem to agree with this interpretation, and shows that cocontraction adapts according to the effect it has on the tracking performance.

The cocontraction may depend on the statistical information determining the quality of the planned motion, which relies primarily on vision, and on the quality of the partner's accuracy in tracking the common target. We propose that the cocontraction is modulated to maximise visual and haptic information from the interaction with the partner. Specifically, the *optimal information and effort* (OIE) model addresses the tradeoff between motion guidance and interaction noise attenuation by selecting cocontraction u to minimize the *prediction error*

$$E(u) \equiv \frac{\sigma_o^2(u)\,\sigma_p^2}{\sigma_o^2(u)+\sigma_p^2} \tag{4.16}$$

and *metabolic cost* u^2, where $\sigma_o(u)$ results from the effect of own visual noise on the arm movement and σ_p from the interaction with the partner. This optimization can be carried

out through gradient descent minimization:

$$u_{new} \equiv -\frac{dE(u)}{du} + (1-\gamma)\,u\,, \quad \gamma > 0\,. \tag{4.17}$$

As suggests Fig. 4-5A, the OIE results in less error to the data as the TEM and MPN models. More importantly, the OIE model predicts the modulation of cocontraction with both own visual noise and haptic noise from the partner as observed in the data (Fig. 4-5B), in contrast to the TEM and PNM models.

4.5 Discussion

It was recently shown that physically interacting individuals tracking the same target can improve their performance by estimating the partner's movement goal and using it to complement own sensory information [48]. The present study extends this finding by demonstrating that individuals adapt their muscle contraction to maximize task information while concurrently minimizing energy. We thought that individuals would stiffen the limbs to compensate for visual noise, and relax cocontraction to attenuate the mechanical perturbations from a partner receiving noisy visual feedback. However, the converse adaptation was observed as the CNS considers the guidance to the planned motion and adapts cocontraction to minimize the effect of visual and haptic noise.

These results could not be explained by a previous model of cocontraction adaptation which considers only the error in the task performance [41], [62], [63]. We also considered a motion planning noise model that decreases cocontraction with increasing visual noise to reduce errors in visual motion guidance, but this model could not explain the modulation of cocontraction with the partner's noise. The only model that could explain how cocontraction changes with both own and the partner's noise was the optimal information and effort model (OIE) in which cocontraction is adapted to maximize information from vision and haptics arising from the interaction with the partner.

The OIE model does a deft balance of three variables. First, it tries to minimize energy on a trial-to-trial basis by reducing superfluous cocontraction. Second, it regulates cocontraction to have stiffer guidance towards the planned motion when vision is sharp. Third, it controls cocontraction depending on the haptic information and guidance coming from the partner's actions. Cocontraction increases when haptic information is valuable, but this act reduces guidance from the partner that may be critical to better performance when vision is noisy. In this sense, the cocontraction is skilfully balanced to extract maximal haptic information while exploiting the guidance potential from the partner.

The OIE model of how the CNS adapt cocontraction to minimize information and energy (OIE) extends previous work on motor learning and adaptation, including those determining the motion plan in the next trial from a history of movements [50], [51]. As this new model considers the limbs' neuromechanics, it can predict the interaction force and the subsequent muscle activity during motion. The OIE also extends optimal and nonlinear adaptive control models [41], [52]–[54], [64] by considering the consequence of action on the acquired sensory information from the environment, closing the loop between the sensory and motor actions.

Previous learning algorithms inspired by the observation of human learning adapt muscles' viscoelasticity to compensate for the interaction with an unknown mechanical environment [41], [62], [63]. While these algorithms are based on the error to the motion plan, the proposed OIE model also considers the haptic information that can be gained from the interaction with the environment, and combines it optimally with other information sources like vision. An important aspect of the OIE is that it considers how motor commands like cocontraction can increase or reduce sensor noise, while traditional stochastic optimal control only considered the one-sided influence of sensory noise on motor actions [53]. The adaptation mechanism of OIE can be implemented on robots and used to optimize their interaction with dynamic environments and human partners in collaborative tasks.

Chapter 5 Conclusion

Touch plays a critical role in a human's life since before birth. For the fetus, the sensory system priorities tactile information over auditory or visual cues [65], while soon after birth the exposure to our parents' touch and physical contact is essential in fostering children's adequate growth and development [66]. As we mature, we progressively refine muscle coordination, thus learning how to properly interact with the environment while extracting relevant information from it. In every task involving touch the body acts as a medium to interact with the environment, yet little is known of the role that the body has in tuning haptic sensing (the synthesis of touch and force) and the related perception.

We began this research on adaptive haptic sensing by investigating the human's CNS capability of modulating body properties, specifically limb viscoelasticity, to adapt the acuity of their senses for augmenting the salience of environmental features, such as when the pupil dilates to increase visual acuity in the dark. Past literature pointed out the CNS ability to control the body's stiffness to shape the mechanical interaction with the environment [29], [42] along with how the coupling mechanics affects the exchange of haptic information during physical interaction [15]. However, it was challenging to show that the haptic sense adapts its sensitivity as the percept (the interaction force) cannot be separated from its mechanical influence. By developing an experimental paradigm wherein robotic motion guidance changed with the participant's muscle activity to disentangle the haptic percept from its mechanical effect, we could demonstrate the CNS' ability to willingly regulate the wrist's stiffness (using muscle coactivation) and so to augment haptic sensitivity when it is congruent with vision, and decreases it when the haptic information is poor. We further proposed a computational adaptive haptic sensing mechanism

that explains the underlying principle of this adaptation, accurately predicting the experimental data and revealing how the CNS optimizes the information gain while concurrently minimising the metabolic cost used to sense the haptic percept in an optimal trade-off of information and energy.

To test potential limitations of this adaptive behaviour, we designed a second experiment in which the task completion is hindered by cocontraction dependant perturbations elicited by the natural muscle activation pattern established by the human body morphology. This study showed that humans conspicuously learn muscle activation patterns maximising interaction benefits while filtering disturbances. This highlights the CNS capability to take advantage of adaptive sensing for optimising interactional information using body morphology.

Finally, we validated our understanding of adaptive haptic sensing by studying how physically interacting humans regulate the body viscoelasticity to improve their visuo-haptic perception. By varying noise in the visual channel in each of the mechanically connected partners, we could observe how they adapt muscle cocontraction to regulate their arm viscoelasticity specifically while coordinating their motions. Surprisingly, our computational model could also explain this mechanism: it appears that cocontraction is adapted to optimally combine haptic information from the interaction with the partner and own vision, thereby improving the prediction of the target position with minimal metabolic cost.

The thesis reveals a fundamental human mechanism for adapting sensing during interaction with the environment or other humans. We believe that these new findings will inspire neuroscientists by sheding a light on the basic mechanisms underlying human interaction. These results can help understanding how humans interact with the environment and selectively retrieve task relevant information from it, thus also potentially improving hand interactions identification by introducing muscle activation mediated features. This understanding of the adaptive sensing mechanism could inspire engineers to conceive soft robots that can modify their rigidity to better perceive the user's control and assist them.

Furthermore, the results of the studies in this thesis may enable the development of more efficient sensorimotor strategies for applications requiring human-robot interaction such as collaborative robots for manufacturing and robot-assisted physical training.

As a following step, the OIE adaptation mechanism could be implemented on a robotic interface to test whether the underlying stiffness adaptation can filter haptic noise to improve the robot's sensing of the interaction and provide its user a more reliable haptic percept. In general, the OIE algorithm could optimize robots physical interactions by identifying the optimal control gain for retrieving tactile cues from dynamic environments and exchanging haptic information with humans. Relevant applications include: scenarios in which the haptic information is exchanged through a tunable virtual coupling with an end-effector, as in teleoperation and robotic assisted surgery; shared driving, where the control is balanced between the driver and the robot based on the available sensors measurements' quality; for moving fleets of semi-autonomous and autonomous cars in a shared network connected through virtual spring being tuned depending on the individual behaviours. Likewise, nautical robots may tune the stiffness of the interaction with the environment to collect valuable information in a dark or murky environment, or medical robots to locate anatomical haptic landmarks and abnormalities in internal organs while integrating multiple sensory feedback during soft tissues palpation. Additionally, robots physically interacting with a human during manufacturing or neurorehabilitation could adjust their stiffness to best combine their own measurement with the plan of the human operator inferred from the interaction.

Bibliography

[1] M. A. Srinivasan, "What is Haptics ?", *Laboratory for Human and Machine Haptics: The Touch Lab*, pp. 1–11, 1995.

[2] S. J. Lederman and R. L. Klatzky, "Haptic perception : a tutorial", *Attention, Perception, & Psychophysics*, vol. 71, no. 7, pp. 1439–1459, 2009. DOI: 10.3758/APP.

[3] A. Kavounoudias, J. P. Roll, J. L. Anton, B. Nazarian, M. Roth, and R. Roll, "Proprio-tactile integration for kinesthetic perception: An fMRI study", *Neuropsychologia*, vol. 46, no. 2, pp. 567–575, 2008, ISSN: 00283932. DOI: 10.1016/j.neuropsychologia.2007.10.002.

[4] A. Frisoli, M. Solazzi, M. Reiner, and M. Bergamasco, "The contribution of cutaneous and kinesthetic sensory modalities in haptic perception of orientation", *Brain Research Bulletin*, vol. 85, no. 5, pp. 260–266, 2011, ISSN: 03619230. DOI: 10.1016/j.brainresbull.2010.11.011.

[5] J. M. Suchoski, A. Barron, C. Wu, Z. F. Quek, S. Keller, and A. M. Okamura, "Comparison of kinesthetic and skin deformation feedback for mass rendering", *Proceedings - IEEE International Conference on Robotics and Automation*, vol. 2016-June, pp. 4030–4035, 2016, ISSN: 10504729. DOI: 10.1109/ICRA.2016.7487593.

[6] R. Johansson and K. J. Cole, "Sensory-motor coordination during grasping and manipulative actions", *Current Opinion in Neurobiology*, vol. 2, no. 6, pp. 815–823, Dec. 1992, ISSN: 09594388. DOI: 10.1016/0959-4388(92)90139-C. [Online]. Available: https://linkinghub.elsevier.com/retrieve/pii/095943889290139C.

[7] T. Iberall and C. L. MacKenzie, "Opposition Space and Human Prehension", in *Dextrous Robot Hands*, New York, NY: Springer New York, 1990, pp. 32–54. DOI: 10.1007/978-1-4613-8974-3{_}2. [Online]. Available: http://link.springer.com/10.1007/978-1-4613-8974-3_2.

[8] J. J. Gibson, "Observations on active touch", *Psychological Review*, vol. 69, no. 6, pp. 477–491, 1962, ISSN: 0033295X. DOI: 10.1037/h0046962.

[9] R. Fagiani, F. Massi, E. Chatelet, Y. Berthier, and A. Akay, "Tactile perception by friction induced vibrations", *Tribology International*, vol. 44, no. 10, pp. 1100–1110, 2011. DOI: https://doi.org/10.1016/j.triboint.2011.03.019. [Online]. Available: http://www.sciencedirect.com/science/article/pii/S0301679X11000740.

[10] B. Delhaye, V. Hayward, P. Lefevre, and J. L. Thonnard, "Texture-induced vibrations in the forearm during tactile exploration", eng, *Frontiers in Behavioral Neuroscience*, vol. 6, p. 37, 2012. DOI: 10.3389/fnbeh.2012.00037.

[11] Y. Shao, V. Hayward, and Y. Visell, "Spatial patterns of cutaneous vibration during whole-hand haptic interactions", *Proceedings of the National Academy of Sciences*, vol. 113, no. 15, pp. 4188–4193, 2016, ISSN: 0027-8424. DOI: 10.1073/pnas.1520866113. [Online]. Available: http://www.pnas.org/lookup/doi/10.1073/pnas.1520866113.

[12] I. Cesini, J. D. Ndengue, E. Chatelet, J. Faucheu, and F. Massi, "Correlation between friction-induced vibrations and tactile perception during exploration tasks of isotropic and periodic textures", *Tribology International*, vol. 120, pp. 330–339, 2018. DOI: https://doi.org/10.1016/j.triboint.2017.12.041. [Online]. Available: http://www.sciencedirect.com/science/article/pii/S0301679X17305996.

[13] L. R. Manfredi, H. P. Saal, K. J. Brown, *et al.*, "Natural scenes in tactile texture", eng, *Journal of Neurophysiology*, vol. 111, no. 9, pp. 1792–1802, 2014. DOI: 10.1152/jn.00680.2013.

[14] Y. Visell, B. L. Giordano, G. Millet, and J. R. Cooperstock, "Vibration influences haptic perception of surface compliance during walking", *PLOS ONE*, vol. 6, no. 3, e17697, 2011. DOI: 10.1371/journal.pone.0017697. [Online]. Available: https://doi.org/10.1371/journal.pone.0017697.

[15] A. Takagi, F. Usai, G. Ganesh, V. Sanguineti, and E. Burdet, "Haptic communication between humans is tuned by the hard or soft mechanics of interaction", *PLOS Computational Biology*, vol. 14, no. 3, A. M. Haith, Ed., e1005971, Mar. 2018, ISSN: 1553-7358. DOI: 10.1371/journal.pcbi.1005971. [Online]. Available: https://dx.plos.org/10.1371/journal.pcbi.1005971.

[16] M. O. Ernst and M. S. Banks, "Humans integrate visual and haptic information in a statistically optimal fashion", *Nature*, vol. 415, no. 6870, pp. 429–433, 2002, ISSN: 00280836. DOI: 10.1038/415429a.

[17] W. Mugge, J. Schuurmans, A. C. Schouten, and F. C. T. van der Helm, "Sensory weighting of force and position feedback in human motor control tasks", *Journal of Neuroscience*, vol. 29, no. 17, pp. 5476–5482, 2009, ISSN: 0270-6474. DOI: 10.1523/JNEUROSCI.0116-09.2009. [Online]. Available: http://www.jneurosci.org/cgi/doi/10.1523/JNEUROSCI.0116-09.2009.

[18] M. O. Ernst and H. H. Bülthoff, "Merging the senses into a robust percept", *Trends in Cognitive Sciences*, vol. 8, no. 4, pp. 162–169, 2004, ISSN: 13646613. DOI: 10.1016/j.tics.2004.02.002.

[19] H. B. Helbig and M. O. Ernst, "Optimal integration of shape information from vision and touch", *Experimental Brain Research*, vol. 179, no. 4, pp. 595–606, 2007, ISSN: 00144819. DOI: 10.1007/s00221-006-0814-y.

[20] G. Orbán and D. M. Wolpert, "Representations of uncertainty in sensorimotor control", *Current Opinion in Neurobiology*, vol. 21, no. 4, pp. 629–635, 2011, ISSN: 09594388. DOI: 10.1016/j.conb.2011.05.026.

[21] S. O. Murray, D. Kersten, B. A. Olshausen, P. Schrater, and D. L. Woods, "Shape perception reduces activity in human primary visual cortex", *Proceedings of the National Academy of Sciences*, vol. 99, no. 23, p. 15 164, 2002. DOI: 10.1073/pnas.192579399. [Online]. Available: http://www.pnas.org/content/99/23/15164.abstract.

[22] A. Noe, *Action in perception*. MIT press, 2004, ISBN: 0-262-14088-8.

[23] R. Bajcsy, "Active perception", *Proceedings of the IEEE*, vol. 76, no. 8, pp. 996–1005, 1988, ISSN: 0018-9219. DOI: 10.1109/5.5968.

[24] R. Pfeifer, M. Lungarella, and F. Iida, "Self-organization, embodiment, and biologically inspired robotics", *Science*, vol. 318, pp. 1088–1093, 2007, ISSN: 0036-8075. DOI: 10.1126/science.1145803.

[25] M. Lungarella and O. Sporns, "Mapping information flow in sensorimotor networks", *PLoS Computational Biology*, vol. 2, no. 10, pp. 1301–1312, 2006, ISSN: 1553734X. DOI: 10.1371/journal.pcbi.0020144.

[26] K. J. Friston, J. Daunizeau, J. Kilner, and S. J. Kiebel, "Action and behavior: a free-energy formulation", *Biological Cybernetics*, vol. 102, no. 3, pp. 227–260, 2010. DOI: 10.1007/s00422-010-0364-z. [Online]. Available: https://doi.org/10.1007/s00422-010-0364-z.

[27] N. Hogan, "Impedance control: an approach to manipulation", *IEEE American Control Conference*, pp. 304–313, 1984, ISSN: 00220434. DOI: 10.1115/1.3140702.

[28] H. Gomi and M. Kawato, "Human arm stiffness and equilibrium-point trajectory during multi-joint movement", *Biological Cybernetics*, vol. 76, no. 3, pp. 163–171, 1997, ISSN: 03401200. DOI: 10.1007/s004220050329.

[29] E. Burdet, R. Osu, D. W. Franklin, T. E. Milner, H. Gomi, and M. Kawato, "The central nervous system stabilizes unstable dynamics by learning optimal impedance", *Nature*, vol. 414, pp. 446–449, 2001.

[30] D. W. Franklin, R. Osu, E. Burdet, M. Kawato, and T. E. Milner, "Adaptation to stable and unstable dynamics achieved by combined impedance control and inverse dynamics model", *Journal of Neurophysiology*, vol. 90, no. 5, pp. 3270–3282, 2003, ISSN: 00223077. DOI: 10.1152/jn.01112.2002.

[31] D. W. Franklin, G. Liaw, T. E. Milner, R. Osu, E. Burdet, and M. Kawato, "Endpoint stiffness of the arm is directionally tuned to instability in the environment", *Journal of Neuroscience*, vol. 27, no. 29, pp. 7705–7716, 2007.

[32] D. W. Franklin, U. So, M. Kawato, and T. E. Milner, "Impedance control balances stability with metabolically costly muscle activation", *Journal of Neurophysiologyiology*, vol. 92, no. 5, pp. 3097–3105, 2004.

[33] L. P. J. Selen, D. W. Franklin, and D. M. Wolpert, "Impedance control reduces instability that arises from motor noise", *Journal of Neuroscience*, vol. 29, no. 40, pp. 12 606–12 616, 2009, ISSN: 02706474. DOI: 10.1523/JNEUROSCI.2826-09.2009.

[34] N. Sornkarn, M. Howard, and T. Nanayakkara, "Internal impedance control helps information gain in embodied perception", in *2014 IEEE International Conference on Robotics and Automation (ICRA)*, IEEE, May 2014, pp. 6685–6690, ISBN: 978-1-4799-3685-4. DOI: 10.1109/ICRA.2014.6907846. [Online]. Available: http://ieeexplore.ieee.org/document/6907846/.

[35] N. Sornkarn, "Morphological Computation in Active Haptic Embodied Perception", Ph.D. dissertation, King's College London, 2016, p. 177. [Online]. Available: https://core.ac.uk/download/pdf/83947890.pdf.

[36] R. C. Oldfield, "The assessment and analysis of handedness: The Edinburgh inventory", *Neuropsychologia*, vol. 9, no. 1, pp. 97–113, 1971, ISSN: 00283932. DOI: 10.1016/0028-3932(71)90067-4.

[37] A. Melendez-Calderon, L. Bagutti, B. Pedrono, and E. Burdet, "Hi5: A versatile dual-wrist device to study human-human interaction and bimanual control", *IEEE International Conference on Intelligent Robots and Systems*, pp. 2578–2583, 2011, ISSN: 2153-0858. DOI: 10.1109/IROS.2011.6048068.

[38] A. Takagi, M. Hirashima, D. Nozaki, and E. Burdet, "Individuals physically interacting in a group rapidly coordinate their movement by estimating the collective goal", *eLife*, vol. 8, pp. 1–19, 2019, ISSN: 2050084X. DOI: 10.7554/eLife.41328.

[39] C. D. Takahashi, R. A. Scheidt, and D. J. Reinkensmeyer, "Impedance control and internal model formation when reaching in a randomly varying dynamical environment", *Journal of Neurophysiology*, vol. 86, no. 2, pp. 1047–1051, 2001, ISSN: 00223077. DOI: 10.1152/jn.2001.86.2.1047.

[40] K. A. Thoroughman and R. Shadmehr, "Electromyographic correlates of learning an internal model of reaching movements", *Journal of Neuroscience*, vol. 19, no. 19, pp. 8573–8588, 1999, ISSN: 02706474. DOI: 10.1523/jneurosci.19-19-08573.1999.

[41] D. W. Franklin, E. Burdet, K. Peng Tee, *et al.*, "CNS learns stable, accurate, and efficient movements using a simple algorithm", *Journal of Neuroscience*, vol. 28, no. 44, pp. 11 165–11 173, 2008, ISSN: 0270-6474. DOI: 10.1523/JNEUROSCI.3099-08.2008. [Online]. Available: http://www.jneurosci.org/cgi/doi/10.1523/JNEUROSCI.3099-08.2008.

[42] N. Hogan, "Adaptive control of mechanical impedance by coactivation of antagonist muscles", *IEEE Transactions on Automatic Control*, vol. 29, no. 8, pp. 681–690, 1984, ISSN: 15582523. DOI: 10.1109/TAC.1984.1103644.

[43] F. Lacquaniti, M. Carrozzo, and N. A. Borghese, "Time-varying mechanical behavior of multijointed arm in man", *Journal of Neurophysiology*, vol. 69, no. 5, pp. 1443–1464, 1993, ISSN: 00223077. DOI: 10.1152/jn.1993.69.5.1443.

[44] S. A. Abad, N. Herzig, S. M. H. Sadati, and T. Nanayakkara, "Significance of the compliance of the joints on the dynamic slip resistance of a bioinspired hoof", *IEEE Transactions on Robotics*, vol. 35, no. 6, pp. 1450–1463, 2019, ISSN: 19410468. DOI: 10.1109/TRO.2019.2930864.

[45] A. Prochazka, "Proprioceptive feedback and movement regulation", in *Comprehensive Physiology*, Hoboken, NJ, USA: John Wiley & Sons, Inc., Jan. 2011, ch. 3. DOI: 10.1002/cphy.cp120103. [Online]. Available: http://doi.wiley.com/10.1002/cphy.cp120103.

[46] S. J. Blakemore, C. D. Frith, and D. M. Wolpert, "Spatio-temporal prediction modulates the perception of self-produced stimuli", *Journal of Cognitive Neuroscience*, vol. 11, no. 5, pp. 551–559, 1999, ISSN: 0898929X. DOI: 10.1162/089892999563607.

[47] D. W. Franklin and D. M. Wolpert, "Specificity of reflex adaptation for task-relevant variability", *Journal of Neuroscience*, vol. 28, no. 52, pp. 14 165–14 175, 2008, ISSN: 02706474. DOI: 10.1523/JNEUROSCI.4406-08.2008.

[48] A. Takagi, G. Ganesh, T. Yoshioka, M. Kawato, and E. Burdet, "Physically interacting individuals estimate the partner's goal to enhance their movements", *Nature Human Behaviour*, vol. 1, no. 3, 2017, ISSN: 23973374. DOI: 10.1038/s41562-017-0054.

[49] J. B. Heald, D. W. Franklin, and D. Wolpert, "Increasing muscle co-contraction speeds up internal model acquisition during dynamic motor learning", *Scientific Reports*, vol. 8, no. 1, pp. 1–11, 2018, ISSN: 20452322. DOI: 10.1038/s41598-018-34737-5.

[50] D. J. Herzfeld, P. A. Vaswani, M. K. Marko, and R. Shadmehr, "A memory of errors in sensorimotor learning", *Science*, vol. 345, no. 6202, pp. 1349–1354, 2014.

[51] K. Takiyama, M. Hirashima, and D. Nozaki, "Prospective errors determine motor learning", *Nature Communications*, vol. 6, pp. 1–12, 2015, ISSN: 20411723. DOI: 10.1038/ncomms6925.

[52] C. M. Harris and D. M. Wolpert, "Signal-dependent noise determines motor planning", *Nature*, vol. 394, no. 6695, pp. 780–784, 1998, ISSN: 00280836. DOI: 10.1038/246170a0.

[53] E. Todorov and M. I. Jordan, "Optimal feedback control as a theory of motor coordination", *Nature Neuroscience*, vol. 5, no. 11, pp. 1226–1235, 2002, ISSN: 10976256. DOI: 10.1038/nn963.

[54] C. Wang, Y. Xiao, E. Burdet, J. Gordon, and N. Schweighofer, "The duration of reaching movement is longer than predicted by minimum variance", *Journal of Neurophysiology*, vol. 116, no. 5, pp. 2342–2345, 2016, ISSN: 15221598. DOI: 10.1152/jn.00148.2016.

[55] M. Lungarella, T. Pegors, D. Bulwinkle, and O. Sporns, "Methods for quantifying the informational structure of sensory and motor data", *Neuroinformatics*, vol. 5, no. 1, pp. 11–34, 2005, ISSN: 1539-2791. DOI: 10.1385/NI. [Online]. Available: http://www.ncbi.nlm.nih.gov/pubmed/17426351.

[56] N. Alva, *Action in Perception*. The MIT Press, 2004, pp. 1–34, ISBN: 0-262-14088-8.

[57] R. F. Kirsch, D. Boskov, and W. Z. Rymer, "Muscle stiffness during transient and continuous movements of cat muscle: perturbation characteristics and physiological relevance", *IEEE Transactions on Biomedical Engineering*, vol. 41, no. 8, pp. 758–770, 1994, ISSN: 15582531. DOI: 10.1109/10.310091.

[58] K. Körding and D. M. Wolpert, "Bayesian integration in sensorimotor learning", *Nature*, vol. 427, no. 6971, pp. 244–247, 2004, ISSN: 00280836. DOI: 10.1038/nature02169.

[59] E. Field and D. Harris, "A comparative survey of the utility of cross-cockpit linkages and autoflight systems' backfeed to the control inceptors of commercial aircraft", *Ergonomics*, vol. 41, no. 10, pp. 1462–1477, 1998, ISSN: 00140139. DOI: 10.1080/001401398186216.

[60] L. P. J. Selen, J. H. Van Dieën, and P. J. Beek, "Impedance modulation and feedback corrections in tracking targets of variable size and frequency", *Journal of Neurophysiology*, vol. 96, no. 5, pp. 2750–2759, 2006, ISSN: 00223077. DOI: 10.1152/jn.00552.2006.

[61] G. Carboni, T. Nanayakkara, A. Takagi, and E. Burdet, "Adapting the visuo-haptic perception through muscle coactivation", *Scientific Reports*, vol. 11, no. 1, p. 21 986, Dec. 2021, ISSN: 2045-2322. DOI: 10.1038/s41598-021-01344-w. [Online]. Available: https://www.nature.com/articles/s41598-021-01344-w.

[62] E. A. Theodorou, J. Buchli, and S. Schaal, "A generalized path integral control approach to reinforcement learning", *Journal of Machine Learning Research*, vol. 11, pp. 3137–3181, 2010, ISSN: 15324435.

[63] Y. Li, G. Ganesh, N. Jarrasse, S. Haddadin, A. Albu-Schaeffer, and E. Burdet, "Force, impedance, and trajectory learning for contact tooling and haptic identification", *IEEE Transactions on Robotics*, vol. 34, no. 5, pp. 1170–1182, 2018, ISSN: 15523098. DOI: 10.1109/TRO.2018.2830405.

[64] W. L. Nelson, "Physical principles for economies of skilled movements", *Biological Cybernetics*, vol. 46, pp. 135–147, 1983, ISSN: 0028-0836. DOI: 10.1038/237055b0.

[65] V. Marx and E. Nagy, "Fetal behavioural responses to maternal voice and touch", *PLoS ONE*, vol. 10, no. 6, pp. 1–15, 2015, ISSN: 19326203. DOI: 10.1371/journal.pone.0129118.

[66] E. L. Ardiel and C. H. Rankin, "The importance of touch in development", *Paediatrics and Child Health*, vol. 15, no. 3, pp. 153–156, 2010, ISSN: 12057088. DOI: 10.1093/pch/15.3.153.